Characterization of Calcium Aluminate Phases in Cements by ^{27}Al MAS NMR Spectroscopy

Jørgen Skibsted,† Eric Henderson,‡ and Hans J. Jakobsen*,†

Department of Chemistry, University of Aarhus, DK-8000 Aarhus C, Denmark, and Euroc Research AB, S-22370 Lund, Sweden

Received June 26, 1992

^{27}Al magic-angle spinning (MAS) NMR spectroscopy of the central and satellite transitions is shown to be a powerful technique for the characterization of calcium aluminates and aluminate hydrates, which are of importance in the chemistry of high alumina and Portland cements. Synthetic samples of $CaO{\cdot}2Al_2O_3$, $CaO{\cdot}Al_2O_3$, $12CaO{\cdot}7Al_2O_3$, $3CaO{\cdot}Al_2O_3$, $CaO{\cdot}Al_2O_3{\cdot}10H_2O$, $3CaO{\cdot}Al_2O_3{\cdot}6H_2O$, γ-$Al(OH)_3$, $6CaO{\cdot}Al_2O_3{\cdot}3SO_3{\cdot}32H_2O$ (ettringite), $4CaO{\cdot}Al_2O_3{\cdot}13H_2O$, $4CaO{\cdot}Al_2O_3{\cdot}SO_3{\cdot}12H_2O$ (monosulfate) and hydrated samples of high alumina and Portland cements are investigated. For the synthetic samples ^{27}Al quadrupole coupling constants (C_Q), asymmetry parameters (η) of the electric field gradient (EFG) tensors, and isotropic chemical shifts ($\delta(^{27}Al)$) are determined with high accuracies from computer simulations of the complete manifolds of spinning sidebands (ssb's) for the satellite transitions or of the central transition (centerband and ssb's). Simulations of the ssb manifolds show that some of the samples cannot be characterized by a single set of C_Q and η values, but rather by a distribution of these values. The ranges of the distributions in C_Q and η are estimated by summation of simulated ssb patterns for the satellite transitions employing sets of slightly different C_Q and η values. The quadrupole coupling parameters are shown to be an important supplement to $\delta(^{27}Al)$ in the characterization of structurally different Al sites and for identification of the individual aluminates in ^{27}Al MAS NMR spectra of hydrated cement samples. Linear correlations between C_Q and the mean bond angle deviation from ideal tetrahedral symmetry, as well as between C_Q and a calculated estimate for the geometrical dependency of the EFG tensor, are reported for the anhydrous calcium aluminates. These correlations allow assignment of the C_Q values for $CaO{\cdot}2Al_2O_3$, $12CaO{\cdot}7Al_2O_3$, and $3CaO{\cdot}Al_2O_3$, all of which contain two nonequivalent AlO_4 tetrahedra in the asymmetric unit.

Introduction

Solid-state nuclear magnetic resonance (NMR) spectroscopy of cement systems has proven to be a valuable technique of studying not only the original anhydrous phases, but also their hydration products using different NMR nuclei (^1H, ^{29}Si, and ^{27}Al) as probes. Early investigations used ^1H NMR,[1] which, when combined with spin-grouping techniques, was used to characterize the hydration behavior by ^1H spin–lattice and spin–spin relaxation times.[2] Advances in magic-angle spinning (MAS) NMR techniques have made ^{29}Si a popular and useful nucleus in studies of cements and other areas of materials science. Lippmaa et al.[3] first used ^{29}Si MAS NMR to investigate the hydration of synthetic tricalcium silicate. They found that the ^{29}Si chemical shifts reflected the degree of condensation of the SiO_4 tetrahedra in the amorphous calcium silicate hydrates. Since these studies ^{29}Si MAS NMR has been widely used to study the hydration behavior of Portland cement systems.[4,5]

In recent years ^{27}Al MAS NMR spectroscopy has achieved considerable success in studies of polycrystalline and amorphous materials from various branches of inorganic chemistry.[6–10] However, only a few applications to cement chemistry have appeared.[5,11–15] Generally, ^{27}Al MAS NMR has been concerned with the distinction between tetrahedrally (Al(4)) and octahedrally (Al(6)) coordinated aluminum, using the distinct chemical shift difference of about 60 ppm for these two types of Al coordination.[16] This has been utilized in ^{27}Al MAS NMR studies of the hydration kinetics of synthetic calcium aluminate ($CaO{\cdot}Al_2O_3 \equiv CA$)[11] and high alumina cement (*HAC*);[13,14] the shorthand cement nomenclature where C = CaO, A = Al_2O_3, S = SiO_2, F = Fe_2O_3, $\bar{S}$ = SO_3, H = H_2O, and D = D_2O is employed throughout this paper. In a preliminary investigation we applied ^{27}Al MAS NMR to the low aluminate content of white Portland cement and proved its potential in following the hydration reactions of the aluminate phase in Portland cements.[5] ^{27}Al chemical shifts (δ) and quadrupole coupling parameters (i.e., the quadrupole coupling constant, $C_Q = e^2qQ/h$, and asymmetry parameter η, $0 \le \eta \le 1$, of the electric field gradient (EFG) tensor) have been

* Author to whom correspondence and inquiries about the paper should be addressed.
† University of Aarhus, Denmark.
‡ Euroc Research AB, Sweden.

(1) (a) Seligmann, P. *J. Res. Dev. Lab. Portland Cem. Assoc.* **1968**, *10*, 52. (b) Blinc, R.; Burgar, M.; Lahajnar, G.; Rozmarin, M.; Rutar, V.; Kocuvan, I.; Ursic, J. *J. Am. Ceram. Soc.* **1978**, *61*, 35.
(2) (a) MacTavish, J. C.; Miljkovic, L.; Pintar, M. M.; Blinc, R.; Lahajnar, G. *Cem. Concr. Res.* **1985**, *15*, 367. (b) Schreiner, L. J.; MacTavish, J. C.; Miljkovic, L.; Pintar, M. M.; Blinc, R.; Lahajnar, G.; Lasic, D.; Reeves, L. W. *J. Am. Ceram. Soc.* **1985**, *68*, 10.
(3) Lippmaa, E.; Mägi, M.; Tarmak, M.; Wieker, W.; Grimmer, A.-R. *Cem. Concr. Res.* **1982**, *12*, 597.
(4) (a) Clayden, N. J.; Dobson, C. M.; Groves, G. W.; Hayes, C. J.; Rodger, S. A. *Proc. Br. Ceram. Soc.* **1984**, *35*, 55. (b) Barnes, J. R.; Clague, A. D. H.; Clayden, N. J.; Dobson, C. M.; Hayes, C. J.; Groves, G. W.; Rodger, S. A. *J. Mater. Sci. Lett.* **1985**, *4*, 1293. (c) Rodger, S. A.; Groves, G. W.; Clayden, N. J.; Dobson, C. M. *J. Am. Ceram. Soc.* **1988**, *71*, 91. (d) Dobson, C. M.; Goberdhan, D. G. C.; Ramsay, J. D. F.; Rodger, S. A. *J. Mat. Sci.* **1988**, *23*, 4108. (e) Macphee, D. E.; Lachowski, E. E.; Glasser, F. P. *Adv. Cem. Res.* **1988**, *1*, 131. (f) Groves, G. W.; Rodger, S. A. *Adv. Chem. Res.* **1989**, *2*, 135. (g) Grutzeck, M.; Benesi, A.; Fanning, B. *J. Am. Ceram. Soc.* **1989**, *72*, 665.
(5) Hjorth, J.; Skibsted, J.; Jakobsen, H. *J. Cem. Concr. Res.* **1988**, *18*, 789.
(6) Lippmaa, E.; Samoson, A.; Mägi, M. *J. Am. Chem. Soc.* **1986**, *108*, 1730.
(7) Engelhardt, G.; Michel, D. *High-Resolution Solid-State NMR of Silicates and Zeolites*; John Wiley & Sons: Chichester, England, 1987.
(8) Woessner, D. E. *Am. Mineral.* **1989**, *74*, 203.
(9) Skibsted, J.; Bildsøe, H.; Jakobsen, H. J. *J. Magn. Reson.* **1991**, *92*, 669.
(10) Skibsted, J.; Nielsen, N. C.; Bildsøe, H.; Jakobsen, H. J. *J. Magn. Reson.* **1991**, *95*, 88.
(11) (a) Müller, D.; Rettel, A.; Gessner, W.; Scheler, G. *J. Magn. Reson.* **1984**, *57*, 152. (b) Rettel, A.; Gessner, W.; Müller, D.; Scheler, G. *Br. Ceram. Trans. J.* **1985**, *84*, 25.
(12) Müller, D.; Gessner, W.; Samoson, A.; Lippmaa, E.; Scheler, G. *Polyhedron* **1986**, *5*, 799.
(13) Skibsted, J. In *Proceedings of the First European Conference on Soft Mineralurgy, Compiegne, France, June 1–3*; 1988; Vol. 2, p 179.
(14) Luong, T.; Mayer, H.; Eckert, H. *J. Am. Ceram. Soc.* **1989**, *72*, 2136.
(15) Kudryavtsev, A. B.; Kouznetsova, T. V.; Pyatkova, A. V. *Cem. Concr. Res.* **1990**, *20*, 407.
(16) Müller, D.; Gessner, W.; Behrens, H.-J.; Scheler, G. *Chem. Phys. Lett.* **1981**, *79*, 59.

0020-1669/93/1332-1013$04.00/0

reported for aluminates in the $CaO–Al_2O_3$ system by Müller et al.[12] However, we note that compared to the results obtained in this investigation, substantial differences in C_Q, η, and δ are observed for some samples examined in that study (vide infra). Solid-state ^{27}Al NMR spectra are generally complicated by second-order quadrupolar shifts and line broadening effects, which may be present even at the highest available magnetic fields. The C_Q and η parameters are extremely sensitive to the EFG's at the nuclear site and can provide valuable information about the distortion and symmetry of the AlO_4 and AlO_6 polyhedra. Therefore, in addition to the correct determination of $\delta(^{27}Al)$, which requires knowledge of C_Q and η (or at least of the product $C_Q(1 + \eta^2/3)^{1/2}$ [17]), the quadrupolar coupling parameters can be particularly useful for the characterization and identification of structurally different Al sites. The term $C_Q(1 + \eta^2/3)^{1/2}$, which governs the degree of the second-order quadrupolar line broadening and shifts at a particular magnetic field, is usually determined from the difference in second-order quadrupolar shifts for the individual transitions.[17,18] For this reason it is generally termed the *second-order quadrupolar effect* parameter (i.e., $SOQE = C_Q(1 + \eta^2/3)^{1/2}$).[8,10,17]

This study reports the determination of ^{27}Al quadrupole coupling parameters and chemical shifts by MAS NMR for calcium aluminates and their hydrates, which are of interest in the chemistry of *HAC* and Portland cements. This includes the first detailed ^{27}Al MAS NMR study of C_4AH_{13} and the sulfate-containing hydrates, ettringite ($C_6A\bar{S}_3H_{32}$), and the monosulfate ($C_4A\bar{S}H_{12}$). A knowledge of the above parameters, for both the individual cement components and their hydration products, is a prerequisite for an unambiguous interpretation of the complex ^{27}Al MAS NMR spectra of cements. Furthermore, it is shown that the individual components are in some instances more conveniently characterized by their C_Q and η values, because of the very limited chemical shift variations observed within the regions for Al(4) and Al(6). This is illustrated by the ^{27}Al MAS NMR spectra of hydrated cements where the calcium aluminate hydrates are easily identified from the spinning sideband (ssb) manifolds for the satellite transitions ($m = \pm^1/_2 \leftrightarrow m = \pm^3/_2$ and $m = \pm^3/_2 \leftrightarrow m = \pm^5/_2$), which reflect the C_Q and η values. Finally, we show that the quadrupole coupling constants for the anhydrous calcium aluminates may be related to the geometry of the first ^{27}Al coordination sphere which allows tentative assignment of the C_Q values for CA_2, $C_{12}A_7$, and C_3A. A variety of NMR methods for determination of quadrupole coupling parameters have recently been developed. These include MAS, VAS, nutation NMR, DOR, DAS, and SQUID techniques (see ref 10 and references cited herein). For the cement samples investigated here, the determination of C_Q and η employed line-shape simulations of the central ($m = ^1/_2 \leftrightarrow m = -^1/_2$) transition at high spinning speeds[9] (for large C_Q's), and/or simulations of the ssb pattern for the satellite transitions[10,17] (for small C_Q's). Both methods result in quadrupole coupling parameters of high accuracy.

Experimental Section

NMR Measurements. Solid-state ^{27}Al MAS NMR spectra were obtained on Varian XL-300 (7.1 T) and VXR-400 S (9.4 T) spectrometers, both connected to a SUN 3/150 computer. A few ^{27}Al MAS NMR spectra were recorded at 11.7 T on a Varian VXR-500 spectrometer. All spectrometers were equipped with homebuilt high-speed spinning MAS probes.[19] Spinning speeds in the range from about 2 to 20 kHz, with accuracies of ±5 Hz, were available using 4, 5, and 7 mm o.d. Si_3N_4 rotors with sample volumes of 77, 130, and 220 μL, respectively.[20] The magic angle was set with an accuracy of ±0.005° by minimizing the line widths of the ssb's from the satellite transitions in the ^{23}Na MAS spectrum of $NaNO_3$.[21] All experiments employed single pulse excitation with pulse widths τ_p = 1–2 μs, rf field strengths $\gamma_1 H_1/2\pi$ = 40–60 kHz, and a 1 s relaxation delay. High-power proton decoupling was applied for the hydrate samples during acquisition of the FID's. Base-line distortions resulting from the spectrometer deadtime were removed using a modified version of the Varian base-line correction routine. ^{27}Al isotropic chemical shifts (δ) are reported in ppm relative to an external sample of 1.0 M $AlCl_3 \cdot 6H_2O$.

Simulation Software. All computer simulations were performed using a general software package developed in our laboratory for simulation of MAS/VAS NMR spectra of quadrupolar nuclei.[9,10,17] The simulations were performed on a Digital VAX 6210 computer or on the SUN 3/150 computer of the VXR-400 S spectrometer. The latter has the advantage that data processing of the simulated spectra may be carried out using all the options of the standard Varian VNMR software. The programs calculate contributions from first- and second-order quadrupolar interactions in the secular approximation and includes effects from nonuniform excitation (i.e., finite rf pulse widths and field strengths) and detection (i.e., quality factor Q of the probe circuit).[10] As reported earlier,[10] the time-consuming calculations of the second-order terms for the satellite transitions (ssb's) can be omitted for weak quadrupolar couplings (i.e., $C_Q \lesssim 4$ MHz for $I = ^5/_2$), since the first-order contribution gives an excellent fit to the ssb intensities. Fitting of the calculated to experimental ssb intensities for the satellite transitions is undertaken by combining the simulation program with the MINUIT[22] optimization routine. In addition to the experimental parameters and integrated ssb intensities, the optimization routine requires initial estimates for C_Q and η. These are conveniently derived from *SOQE* in combination with the numerical frequency (ν_i) of the inner singularities.[10] The *SOQE* parameter may be obtained from differences in second-order quadrupolar shift for the individual ^{27}Al transitions.[17,18] However, for very weak quadrupolar interactions (i.e., $C_Q \lesssim 0.5$ MHz) we have found that the *SOQE* parameter may be determined with higher accuracy from moment analysis. The second moment for the quadrupole interaction includes the *SOQE* parameter and is given by[23]

$$M_2 = \sum_m p_m M_{2m} \tag{1}$$

In this expression M_{2m}, the second moment for the $(m, m-1)$ transition, is given by

$$M_{2m} = \frac{9(1-2m)^2 SOQE^2}{80I^2(2I-1)^2} \tag{2}$$

and

$$p_m = \frac{3[I(I+1) - m(m-1)]}{2I(I+1)(2I+1)} \tag{3}$$

is the corresponding squared transition probability. Experimentally M_2 is determined from centerbands and ssb intensities according to[23]

$$M_2 = \nu_r^2 \sum_{-n}^{+n} n^2 I_n / \sum_{-n}^{+n} I_n \tag{4}$$

where I_n is the intensity of the nth ssb (I_0 is the centerband intensity) and ν_r is the spinning frequency.

Materials. The basic structure and purity of all the synthetic samples studied was checked by X-ray powder diffraction using the JCPDS diffraction files. Synthetic samples of the calcium aluminates were obtained from Lafarge, Viviers, France (CA and CA_2) and Aalborg Portland, Aalborg, Denmark (C_3A and $C_{12}A_7$) whilst γ-AH_3 (extra pure grade) was obtained from Merck. CAH_{10} was prepared by hydration of finely powdered CA in an excess of water at 5 °C.[24] The sample was

(17) Jakobsen, H. J.; Skibsted, J.; Bildsøe, H.; Nielsen, N. C. *J. Magn. Reson.* **1989**, *85*, 173.
(18) Samoson, A. *Chem. Phys. Lett.* **1985**, *119*, 29.
(19) Jakobsen, H. J.; Daugaard, P.; Langer, V. *J. Magn. Reson.* **1988**, *76*, 162; U.S. Patent Number 4, 739,270, April 19, 1988.
(20) Daugaard, P.; Langer, V.; Jakobsen, H. J. Presented at the 31st Experimental NMR Conference, Asilomar, CA, 1990; Poster WP 20.
(21) Jakobsen, H. J.; Langer, V.; Daugaard, P.; Bildsøe, H. Presented at the 31st Experimental NMR Conference, Asilomar, CA, 1990, Poster WP 19.
(22) James, F.; Ross, M. MINUIT Computer Code, CERN, Geneva, Program D-506; *Comput. Phys. Commun.* **1975**, *10*, 343.
(23) Maricq, M. M.; Waugh, J. S. *J. Chem. Phys.* **1979**, *70*, 3300.
(24) Buttler, F. G.; Taylor, H. F. W. *Cemento* **1978**, *75*, 147.

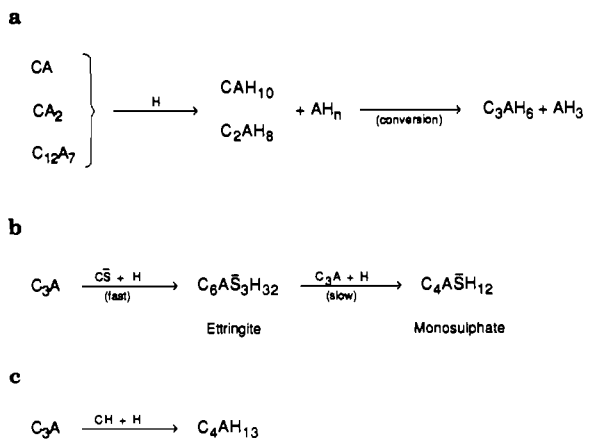

Figure 1. Hydration schemes for the most important calcium aluminates shown in part a for high alumina cement (*HAC*) and in parts b and c for Portland cement. Parts b and c correspond to the hydration of C_3A in Portland cement in the presence and absence of calcium sulfate, respectively. Note the shorthand cement nomenclature: C = CaO, A = Al_2O_3, $\bar{S}$ = SO_3, and H = H_2O.

shaken frequently and the hydration stopped after about 3 weeks, and the sample was filtered and dried at 20 °C. X-ray powder diffraction of the CAH_{10} sample indicated, in agreement with its ^{27}Al MAS NMR spectrum (vide infra), a minor impurity of CA. No reflections corresponding to hydrates such as C_2AH_8 and AH_3 were observed. Ettringite ($C_6A\bar{S}_3H_{32}$) was prepared by the suspension hydration of pure C_3A in calcium sulfate. After 60 days of continuous stirring, the suspension was filtered, washed with a little water and then acetone, and dried over silica gel. Monosulfate ($C_4A\bar{S}H_{12}$) was prepared by adding with stirring stoichiometric quantities of saturated calcium hydroxide and calcium sulfate to a solution of sodium aluminate. The suspension was stirred for 5 min and then filtered after 30 min, washed with alcohol, and dried over silica gel. C_4AH_{13} was prepared by adding an excess of saturated calcium hydroxide (25% more than stoichiometric) to a solution of sodium aluminate at 20 °C and then leaving it overnight at 5 °C. The solid was obtained by vacuum filtering, washing with acetone/water (1/1) in a N_2 filled glove box, and drying in a desiccator over SiO_2 gel. Ettringite, monosulfate, and C_4AH_{13} were analyzed by X-ray diffraction and found to be close to 95% pure. The monosulfate was found to be particularly difficult to prepare, and only when the overall preparative conditions were correct was this phase obtained with the above purity. The high alumina cement (*HAC*), Alcoa-CA-14 (70.4% (w) Al_2O_3, 27.1% (w) CaO, 0.3% (w) SiO_2, 0.2% (w) MgO, 0.2% (w) Na_2O, and 0.05% (w) Fe_2O_3), was obtained from the Alcoa Co. Standard works' ordinary Portland cement (63.4% (w) CaO, 19.5% (w) SiO_2, 4.2% (w) Al_2O_3, 2.2% (w) Fe_2O_3, 3.5% (w) MgO, 1.08% (w) K_2O, 0.32% (w) Na_2O, and 3.07% (w) SO_3) was obtained from Cementa AB, Sweden. The hydration reactions for the powdered cements were carried out as previously described for other cement samples.[5,13]

Results and Discussion

HAC and Portland cements represent highly complex materials composed mainly of phases within the CaO–Al_2O_3 and CaO–SiO_2 systems. The additional constituent oxides not only form further complex phases, but also enter the various crystalline lattices as impurity ions. In Portland cement most of the SO_3 exists as calcium sulfate, which is added to the clinker during the grinding stage. All of the constituent phases and impurity ions, etc. can affect the overall hydration behavior and the physical–mechanical properties of hardened cement.[25] The hydration reactions of the main aluminate phases in *HAC* and Portland cements are schematically summarized in Figure 1. The overall reaction behavior depends on such variables as the temperature, cement composition, and cement/water ratio, and typically the reaction times range from a few hours to several years. Identification and quantification of the Al phases in hydrated cement samples may be achieved by ^{27}Al MAS NMR, provided spectral features and accurate NMR data (e.g., C_Q, η, and δ) are known for the individual components. The following accurate data for the synthetic phases of the main Al-containing phases and their hydration products, in both *HAC* and Portland cement, are reported and discussed on basis of high-performance ^{27}Al MAS NMR experiments. The ^{27}Al quadrupole coupling parameters and isotropic chemical shifts determined from these experiments are summarized in Table I.

Table I. ^{27}Al Quadrupolar Coupling Constants (C_Q), Asymmetry Parameters (η), and Isotropic Chemical Shifts (δ) for Synthetic Aluminates in Portland and High Alumina Cements

compound		C_Q (MHz)	η	δ (ppm)
CA_2	Al(1)	6.25 ± 0.05	0.88 ± 0.02	75.5 ± 0.5
	Al(2)	9.55 ± 0.05	0.82 ± 0.02	69.5 ± 0.5
CA[a]	Al(1)	2.50	0.20	81.9
	Al(2)	2.60	0.75	83.8
	Al(3)	2.60	0.95	86.2
	Al(4)	3.32	0.53	82.7
	Al(5)	3.37	0.39	81.6
	Al(6)	4.30	0.47	81.2
$C_{12}A_7$	Al(1)	9.7 ± 0.2	0.40 ± 0.10	85.9 ± 1.0
	Al(2)	3.8 ± 0.2	0.70 ± 0.10	80.2 ± 0.3
C_3A	Al(1)	8.69 ± 0.05	0.32 ± 0.02	79.5 ± 0.5
	Al(2)	9.30 ± 0.05	0.54 ± 0.02	78.3 ± 0.5
CAH_{10}		2.4 ± 0.2[b]		10.2 ± 0.3
C_3AH_6		0.705 ± 0.010	0.09 ± 0.02	12.36 ± 0.06
C_4AH_{13}		1.8 ± 0.2[b]		10.2 ± 0.2
γ-AH_3	Al(1)	1.97 ± 0.07	0.73 ± 0.04	10.4 ± 0.3
	Al(2)	4.45 ± 0.05	0.44 ± 0.03	11.5 ± 0.3
$C_6A\bar{S}_3H_{32}$		0.360 ± 0.010	0.19 ± 0.03	13.1 ± 0.1
$C_4A\bar{S}H_{12}$		1.7 ± 0.2[b]		11.8 ± 0.2

[a] Tentative C_Q, η, and δ values for the six Al sites in CA obtained from simulation of the centerband for the central transition at 7.1 T and 9.4 T with six overlapping centerband lineshapes (see Figure 5a–h). The indexing of the Al sites is not related to the structure reference. C_Q, η, and δ values for the Al(1) and Al(2) sites are in reasonable agreement with $SOQE$ = 2.6 ± 0.5 MHz, δ = 81.0 ± 0.5 ppm, and $SOQE$ = 2.7 ± 0.5 MHz, δ = 83.6 ± 0.5 ppm, respectively, which are determined from the ssb's at 7.1 T and 9.4 T, using the field-dependence of the center of gravities for ($\pm^3/_2$, $\pm^1/_2$) satellite transitions. [b] Second-order quadrupolar effect parameter ($SOQE = C_Q(1 + \eta^2/3)^{1/2}$) obtained from the frequency-shifts of the center of gravities for the central and ($\pm^3/_2$, $\pm^1/_2$) satellite transitions.

High Alumina Cement (*HAC*) Components. The calcium aluminates CA, CA_2, and $C_{12}A_7$ constitute the predominating phases in high alumina cements.[25] During hydration of *HAC* (Figure 1a), the initially formed hydration products are the metastable hydrates CAH_{10}, C_2AH_8, and alumina gel (AH_n). On standing, CAH_{10} and C_2AH_8 convert into the thermodynamically stable hydrate C_3AH_6, and the alumina gel tends to crystallize into gibbsite (γ-AH_3).[24]

CA_2. The ^{27}Al MAS NMR spectrum of calcium dialuminate (CA_2) recorded at 9.4 T and using a spinning speed ν_r = 18.0 kHz is illustrated in Figure 2. Ultrahigh-speed spinning is required for this aluminate at 9.4 T in order to observe the central transition centerband without distortion or overlap from its first-order ssb's. As recently demonstrated,[9] this facilitates and may be a prerequisite for a correct spectral simulation of the centerband lineshape. Expansion of the line shape in Figure 2b displays two overlapping centerbands corresponding to two tetrahedrally coordinated Al sites. The two inner singularities observed for each of the two lineshapes are readily assigned to the individual Al resonances, and initial estimates for C_Q, η, and δ may be arrived at in combination with the frequencies observed for other singularities, shoulders, or edges. Refinements of these parameters by optimizing the simulations for the two second-order quadrupolar lineshapes (Figure 2d,e) lead to the following parameters for the two Al sites: C_Q = 6.25 ± 0.05 MHz, η = 0.88 ± 0.02, δ_{iso} = 75.5 ± 0.5 ppm for Al(1) (Figure 2e), and C_Q = 9.55 ± 0.05 MHz, η = 0.82 ± 0.02, δ_{iso} = 69.5 ± 0.5 ppm for

(25) Taylor, H. F. W. *Cement Chemistry*; Academic Press Ltd.: London, 1990.

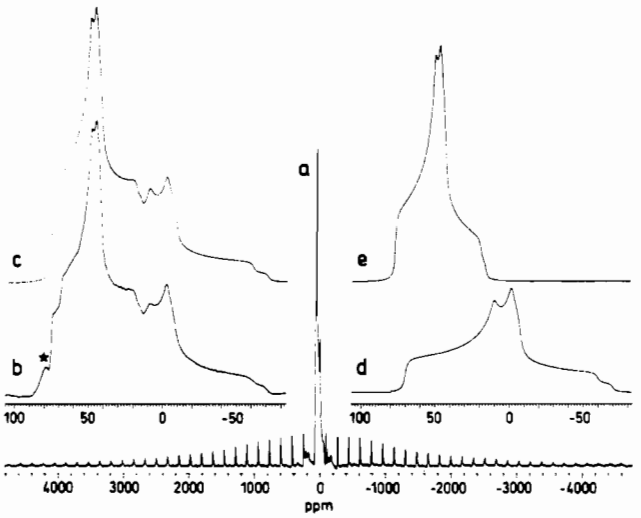

Figure 2. ^{27}Al MAS NMR spectra of CA_2 obtained at 104.2 MHz (9.4 T) using ν_r = 18.0 kHz. (a) Experimental spectrum (1 MHz spectral width) illustrating the centerband for the central transition as well as ssb's from the central and satellite transitions. (b) Expansion of the centerband from the central transition in part a where the asterisk indicates the centerband for the ($\pm^3/_2$, $\pm^1/_2$) satellite transitions. The optimum simulated centerband line shape for the two Al sites in CA_2 is shown in c, while parts d and e illustrate simulated lineshapes for the individual Al sites. Part d corresponds to C_Q = 9.55 MHz, η = 0.82, and δ = 69.5 ppm, and part e, to C_Q = 6.25 MHz, η = 0.88, and δ = 75.5 ppm.

Al(2) (Figure 2d). The combined simulated line shape, resulting from the two sites, is shown in Figure 2c which is in excellent agreement with the experimental spectrum (Figure 2b). Experimental and simulated ^{27}Al MAS NMR spectra at magnetic field strengths of 7.1 T (78.2 MHz, ν_r = 18.2 kHz) and 11.7 T (130.2 MHz, ν_r = 15.2 kHz) are shown in Figure 3 and were performed in order to confirm the parameters determined at 9.4 T (Figure 2). The same parameters (C_Q, η, and δ) as obtained at 9.4 T (Table I) have been employed for the simulations of the spectra at 7.1 T (Figure 3a) and 11.7 T (Figure 3c) which include the central transition, the ($\pm^1/_2$, $\pm^3/_2$) satellite transitions, and their ssb's. From simulations of the line shapes for the ssb's from the ($\pm^1/_2$, $\pm^3/_2$) transitions, it appears that the 11.7 T spectrum is recorded slightly off the magic-angle of θ = 54.74°, as illustrated by the vertically expanded ssb's in Figure 3e–g. Simulations with systematic variations of θ within θ = 54.74° ± 0.2° (simulations not shown) indicate that the line shapes of the ssb's are very sensitive to small deviations from the magic angle and that the experimental spectrum (Figure 3d) corresponds to an angle θ = 54.86° (c.f. Figure 3e–g). Furthermore, it is observed that deviations larger than ca. 0.2° from the magic angle may be used to suppress the resonances from the satellite transitions. Comparison of the ^{27}Al MAS spectra at 7.1, 9.4, and 11.7 T demonstrates the expected reduction in the width of the centerband for the central transition at increasing magnetic field strengths. At high fields this reduces the demand for very high spinning speeds in order to obtain line shapes for the centerband without distortions. The observation of two tetrahedrally coordinated Al atoms is in agreement with the reported crystal structure for CA_2,[26] which is illustrated in Figure 4. The main difference between the two Al sites is that Al(2) is bonded to two tricoordinated oxygen atoms (O(4) in Figure 4) while the Al(1)O_4 tetrahedron only contains one tricoordinated oxygen. The presence of such tricoordinated oxygens adjacent to Al(1) and Al(2) may explain the rather large C_Q values for these two Al sites in CA_2 and also the assignment (vide infra) C_Q(Al(2)) > C_Q(Al(1)).

(26) Ponomarev, V. I.; Kheiker, D. M.; Belov, N. V. *Kristallografija* **1970**, *15*, 1140.

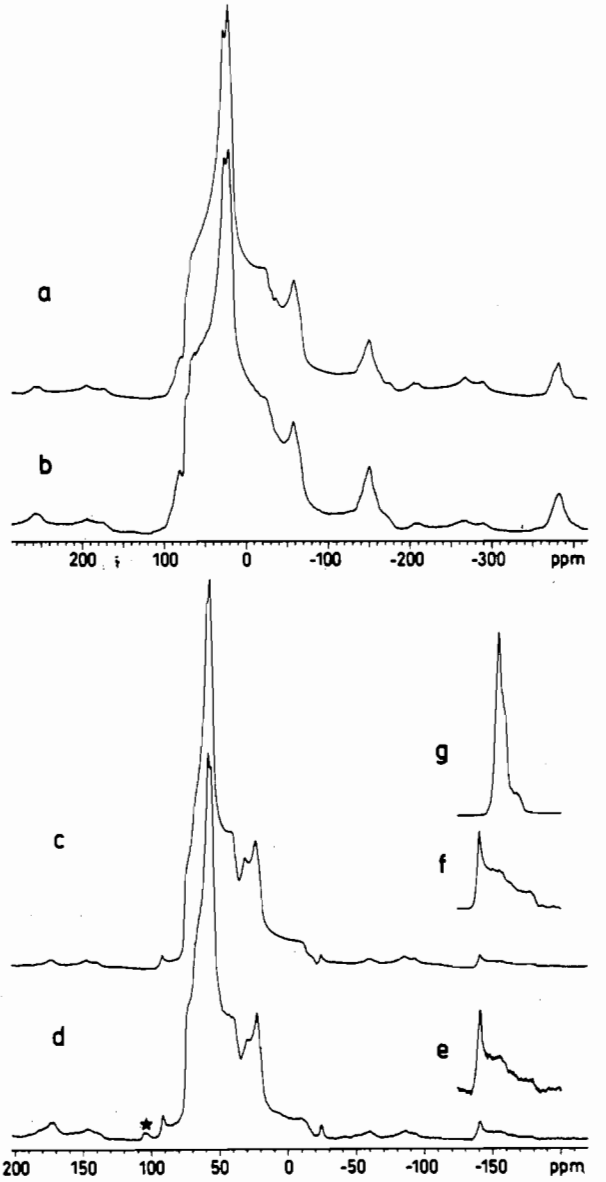

Figure 3. ^{27}Al MAS NMR spectra of CA_2 recorded at (b) 7.1 T and (d) 11.7 T using spinning speeds of ν_r = 18.2 and 15.2 kHz, respectively. Simulated spectra at (a) 7.1 T and (c) 11.7 T of the central and ($\pm^1/_2$, $\pm^3/_2$) transitions, for the two Al sites in CA_2 were obtained, employing the same C_Q, η, and δ values as obtained at 9.4 T (Figure 2). The 11.7-T spectrum is recorded slightly off the magic angle, which is apparent from the vertically expanded ssb's in parts g, e, and f. The simulated ssb in part g corresponds exactly to the magic angle (θ = 54.74°), while the best agreement with the line shape for the experimental ssb's (e) is obtained for θ = 54.86° as shown in part f. The asterisk in part d indicates an Al impurity (Al–N) from the Si_3N_4 rotor material.

^{27}Al quadrupole coupling and chemical shift parameters for CA_2, determined from static and MAS ^{27}Al NMR spectra, have recently been reported by Müller et al.[12] (Al(1), C_Q = 6.7 MHz, η = 0.8, δ = 78 ppm; Al(2), C_Q = 13 MHz, η = 0.1, δ = 60 ppm). The significant discrepancies between these values and those reported here are most likely caused by insufficient resolution, combined with incorrect assignments (static spectrum), and the observation of distorted central transitions (MAS NMR spectrum) as a consequence of using too low a spinning speed (ν_r < 7 kHz at 11.7 T) in the earlier study.[12]

CA. Monocalcium aluminate (CA) constitutes the principal phase of *HAC*. Experimental ^{27}Al MAS NMR spectra of CA obtained at 7.1 T (ν_r = 8.1 kHz) and 9.4 T (ν_r = 8.0 kHz) are shown in parts a and i of Figure 5, respectively. The complex line shape of the centerband for the central transitions (Figure 5a (7.1 T) and Figure 5i (9.4 T)), as well as the shape of the

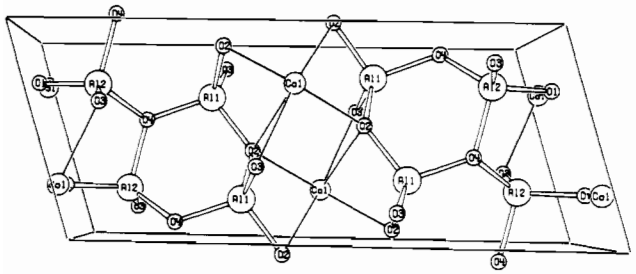

Figure 4. ORTEP projection of the CA_2 structure on the *ac* plane obtained using the reported atomic coordinates.[26] CA_2 is monoclinic with space group $C2/c$ or Cc containing four $CaO{\cdot}2Al_2O_3$ units in the unit cell.[26] Only half of the Al atoms in the cell are included in the projection.

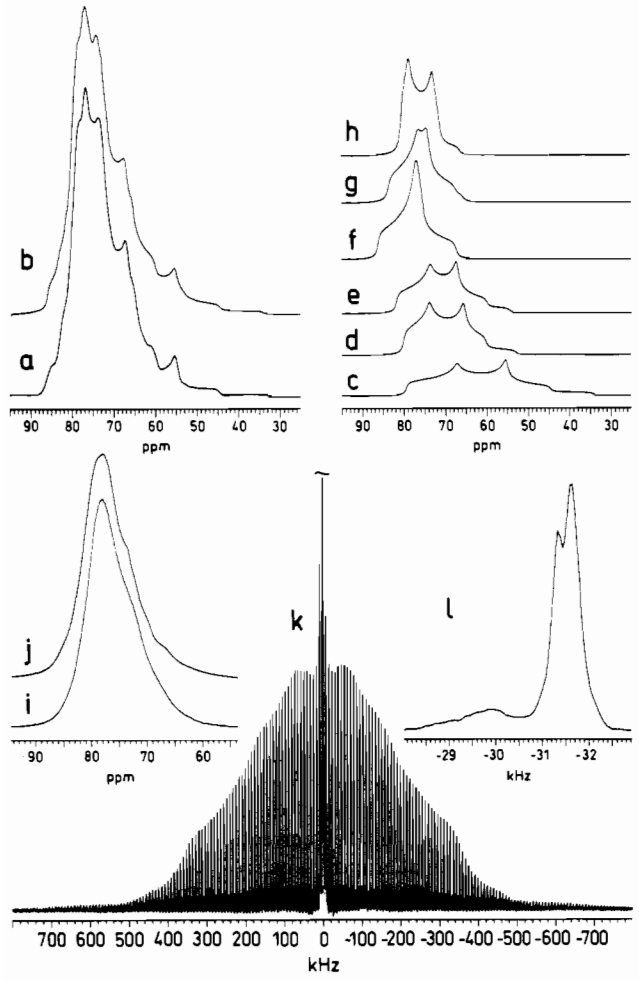

Figure 5. ^{27}Al MAS NMR spectra of CA recorded at (a) 7.1 T and (i,k) 9.4 T employing spinning speeds of ν_r = 8.1 kHz and 8.0 kHz, respectively. (a) Expansion of the centerband from the central transition at 7.1 T. The best simulated centerband line shape we have achieved for the six Al sites in CA is shown in part b. Simulated line shapes at 7.1 T for the individual Al sites are shown in parts c–h which correspond to the C_Q, η, and δ values in Table I: (c) Al(6); (d) Al(5); (e) Al(4); (f) Al(3); (g) Al(2); (h) Al(1). (i) Expansion of the centerband from the central transition at 9.4 T. (j) The corresponding simulated centerband, obtained using the same C_Q, η and δ values for the six Al sites as in part b. (k) Experimental spectrum illustrating the envelope of ssb's from the six Al sites in CA. As shown by the expansion in part l each ssb splits into two peaks from the ($\pm^1/_2$, $\pm^3/_2$) satellite transitions, while the broad resonance at higher field corresponds to overlapping ssb's from the ($\pm^3/_2$, $\pm^5/_2$) satellite transitions.

ssb-manifold from the satellite transitions (Figure 5k), must be attributed to overlapping resonances from several Al sites in CA with quite similar quadrupolar couplings and chemical shifts. This is in accordance with the crystal structure of CA containing six nonequivalent AlO_4 tetrahedra in the asymmetric unit.[27] Approximate values of *SOQE* and δ for two of the Al sites may be obtained from the ssb's of the satellite transitions, which split into two peaks as shown in Figure 5l (9.4 T). Using these splittings and the field-dependence of the center of gravity for the ($\pm^3/_2$, $\pm^1/_2$) transitions gives *SOQE* = 2.6 ± 0.5 MHz, δ = 81.0 ± 0.5 ppm, and *SOQE* = 2.7 ± 0.5 MHz, δ = 83.6 ± 0.5 ppm for at least two of the Al sites. Tentative C_Q, η, and δ parameters, giving an estimate of the quadrupolar couplings in CA, have been obtained from simulations of the experimental centerbands at 7.1 and 9.4 T and for the observed ssb manifold. These simulations for the centerbands are illustrated in Figure 5b,j and represent the best result we were able to achieve using the C_Q, η, and δ parameters for six different overlapping Al resonances (i.e., a total of 18 parameters) shown in Table I. The simulated centerband at 7.1 T is composed of the individual simulated line shapes shown in Figure 5c–h, corresponding to the C_Q, η, and δ data in Table I. An unambiguous determination of C_Q, η and δ values for the six Al sites in CA may hardly be obtained from computer simulation of the experimental centerband at 7.1 T alone, because of (i) the large number of overlapping Al sites, (ii) the insufficient resolution of singularities, shoulders and edges in the second-order quadrupolar lineshapes for each Al site, and (iii) the relatively small variations in quadrupolar coupling as well as chemical shift parameters. Reasonable agreement between the experimental and simulated centerbands is probably also achievable for other sets of quadrupolar coupling and chemical shift values for the Al sites in CA. However, the large number of shoulders and edges observed for the centerband line shape at 7.1 T (Figure 5a) demonstrates that the centerband cannot be simulated using only a single set of C_Q, η, and two δ values as performed by Müller et al.[12] The C_Q, η, and δ parameters, from the simulations in Figure 5, indicate that the variations in the geometry of the six AlO_4 tetrahedra are to a greater degree reflected by C_Q and η, as compared to the chemical shifts. In principle higher resolution of the singularities in the centerband line shape for CA may be obtained at lower magnetic fields. However, the double rotation (DOR)[28,29] and dynamic-angle spinning (DAS)[30] methods appear to be the optimum techniques for verifying the data used for the simulation in Figure 5. Unfortunately, these techniques are not yet available in our laboratory.

$C_{12}A_7$. In high alumina cement $C_{12}A_7$ is generally present as a minor aluminate phase. Figure 6a illustrates the ^{27}Al (104.2 MHz) MAS NMR spectrum of synthetic $C_{12}A_7$, obtained using high-speed spinning (ν_r = 17.8 kHz) and a spectral width of 2 MHz. In agreement with the crystal structure[31] of $C_{12}A_7$ the centerband for the central transition (Figure 6b) displays a line shape corresponding to two different tetrahedrally coordinated Al sites. The ssb manifold observed for the satellite transitions over a spectral width of ca. 1.5 MHz corresponds to the centerband for the narrow resonance at ca. 73 ppm and is assigned to the Al site (Al(2)) with the smallest quadrupolar coupling. The broad centerband ranging from ca. −50 ppm to +80 ppm is ascribed to the centerband for an AlO_4 tetrahedron (Al(1)) with a considerably larger C_Q value. No ssb's are observed for the satellite transitions from this site. Optimization of simulated to integrated ssb intensities for the Al(2) site in $C_{12}A_7$ results in the optimum simulated spectrum shown in Figure 6f, which corresponds to C_Q = 3.8 ± 0.2 MHz, η = 0.70 ± 0.10, and δ = 80.2 ± 0.3 ppm. Employing these parameters for the Al(2) site in the simulations of the partly overlapping centerbands for the central transitions of the Al(1) and Al(2) sites at 9.4 T (Figure 6b) gives the following

(27) Hörkner, W.; Müller-Buschbaum, Hk. *J. Inorg. Nucl. Chem.* **1976**, *38*, 983.
(28) Wu, Y.; Sun, B. Q.; Pines, A.; Samoson, A.; Lippmaa, E. *J. Magn. Reson.* **1990**, *89*, 297.
(29) Chmelka, B. F.; Mueller, K. T.; Pines, A.; Stebbins, J. Wu, Y.; Zwanziger, J. W. *Nature* **1989**, *339*, 42.
(30) Mueller, K. T.; Sun, B. Q.; Chingas, G. C.; Zwanziger, J. W.; Terao, T.; Pines, A. *J. Magn. Reson.* **1990**, *86*, 470.
(31) Bartl, H.; Scheller, T. *Neues Jahrb. Mineral. Monatsh.* **1970**, 547.

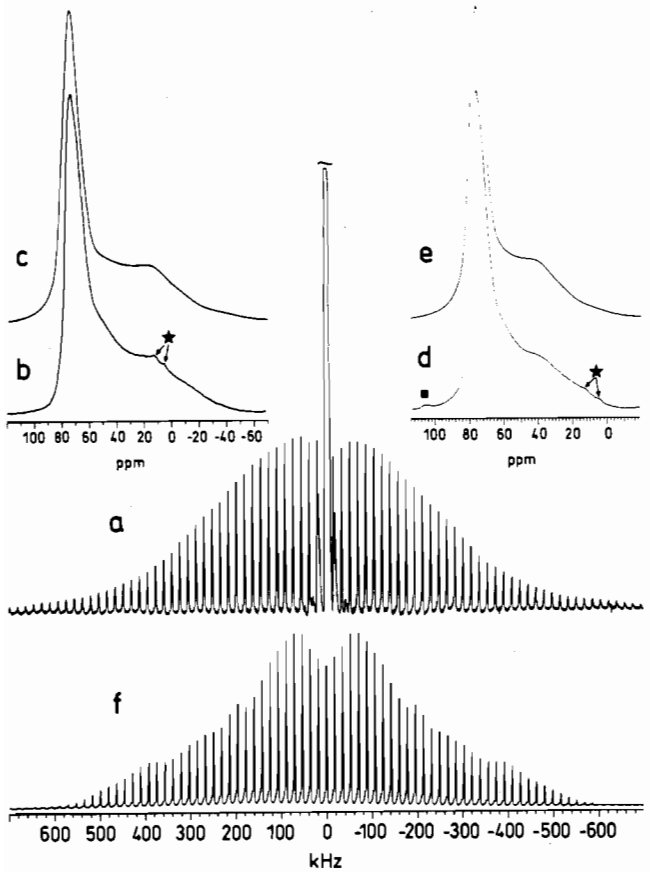

Figure 6. ^{27}Al MAS NMR spectra of $C_{12}A_7$ recorded at (a, b) 9.4 T and (d) 11.7 T using spinning speeds of ν_r = 17.8 kHz and 14.9 kHz, respectively. (a) Experimental spectrum illustrating the central and satellite transitions for the two Al sites in $C_{12}A_7$. (b) Expansion of the centerband for the central transition in part a. (c) Optimum simulated centerband line shape at 9.4 T, for the two Al sites in $C_{12}A_7$, employing C_Q = 9.7 MHz, η = 0.40, and δ = 85.9 ppm for Al(1) and C_Q = 3.8 MHz, η = 0.7, and δ = 80.2 ppm for Al(2). (d) Experimental spectrum of the centerband for the central transition at 11.7 T. (e) The corresponding simulated spectrum employing the same parameters for the Al sites as in part c. The asterisks in parts b and d indicate minor quantities of hydrated material in the sample, and the square in part d indicates an Al impurity (Al–N) from the Si_3N_4 rotor material. (f) Simulated ssb manifold for the satellite transitions for the Al(2) site using the same C_Q, η parameters as in part c. The simulated spectrum includes contributions from the first- and second-order quadrupolar terms and employs Gaussian line broadenings of 1000 and 5000 Hz for the ($\pm^1/_2$, $\pm^3/_2$) and ($\pm^3/_2$, $\pm^5/_2$) transitions, respectively, in order to match the line width observed for the ssb's in part a.

quadrupole couplings and chemical shift values for Al(1): C_Q = 9.7 ± 0.2 MHz, η = 0.40 ± 0.10, and δ = 85.9 ± 1.0 ppm. The simulated spectrum of the centerbands at 9.4 T is shown in Figure 6c and employed an 4:3 intensity ratio for the Al(1) and Al(2) sites, respectively, in agreement with the crystal structure.[31] An experimental ^{27}Al MAS NMR spectrum recorded at 11.7 T (ν_r = 14.9 kHz) of the central transitions in $C_{12}A_7$ is shown in Figure 6d and the corresponding simulated spectrum (Figure 6e) confirms the C_Q, η, and δ values obtained at 9.4 T. The relatively low accuracy of the C_Q, η, and δ values is due to the line broadening observed for the central transitions. The additional line broadening of the central transitions may reflect a small distribution of the C_Q, η, and δ values, resulting from crystal imperfections and/or disorder in the $C_{12}A_7$ sample. These structural effects are also reflected in the ssb pattern observed for the satellite transitions for the Al(2) site (Figure 6a), which appears to be slightly smeared out compared to the simulated ssb manifold. Obviously, improved agreement between simulated and experimental spectra may be obtained by addition of spectra with a slight variation in the C_Q and η values (vide infra). The C_Q, η, and δ values agree reasonably well with those determined from a ^{27}Al NMR investigation of a static powder by Müller et al.[12] (Al(1): C_Q = 11 MHz, η = 0.2, δ = 85 ppm, and C_Q = 3.7 MHz, η = 0.9, δ = 79 ppm).

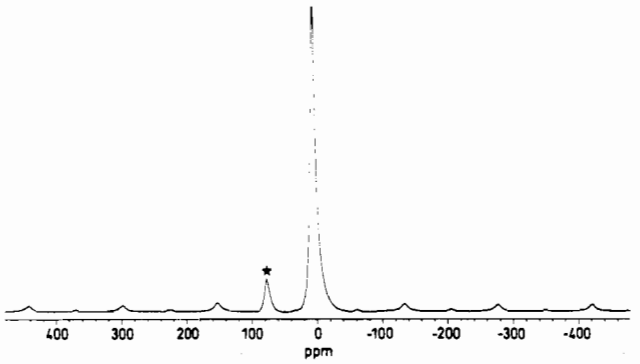

Figure 7. ^{27}Al (104.2 MHz) MAS NMR spectrum of CAH_{10}, obtained using ν_r = 15.0 kHz and ^{1}H decoupling, illustrating the central transition centerband as well as a few ssb's from the satellite transitions. A sample impurity is observed by the centerband resonance at 79 ppm (asterisk) and by the weak ssb's between the ssb's from CAH_{10}. The impurity is identified as CA, and from the relative intensities of the centerband resonances for CAH_{10} and CA it is estimated that CA constitutes 4.0 ± 1.0% (w) of the sample. *SOQE* = 2.4 ± 0.2 MHz and δ = 10.2 ± 0.3 ppm are determined from the spectrum.

CAH_{10}. Hydration of *HAC* at ambient temperature initially leads to the formation of the metastable monocalcium aluminate decahydrate (CAH_{10}).[24] The 9.4-T ^{27}Al MAS NMR spectrum of CAH_{10} (Figure 7), obtained using ν_r = 15.0 kHz and ^{1}H decoupling, displays a featureless and rather broad centerband resonance (full width at half-maximum, fwhm = 7.7 ppm) from the octahedrally coordinated Al site. At a lower spinning speed (ν_r = 2.8 kHz) line widths for the centerband of fwhm = 7.7 ppm and fwhm = 25.6 ppm are observed in spectra with and without ^{1}H decoupling, respectively. It should be noted that spectra recorded without ^{1}H decoupling exhibit a decrease in fwhm with increasing ν_r. Spinning sidebands from the satellite transitions are observed over a spectral range of ca. 1 MHz (not shown), but with no characteristic shape for the ssb-envelope. The difference in quadrupolar shift between the center of gravities for the central and ($\pm^3/_2$, $\pm^1/_2$) transitions allows determination of *SOQE* = 2.4 ± 0.2 MHz, which leads to an approximate value for the quadrupolar coupling (1.9 MHz ≤ C_Q ≤ 2.6 MHz) for the Al site in CAH_{10}. Using *SOQE* a "corrected" chemical shift of δ = 10.2 ± 0.3 ppm is obtained. The *SOQE* and δ values are confirmed from ^{27}Al MAS NMR spectra obtained at 7.1 T. The "bell-shaped" appearance observed for the envelope of the ssb's (similar to that for $C_{12}A_7$ in Figure 6) is ascribed to small variations in the local geometry of the AlO_6 octahedra within the sample, leading to a dispersion in the quadrupole coupling and chemical shift parameters. Thus, the *SOQE* and δ values determined here represent averaged values for the sample. The crystal structure of CAH_{10} is unknown, however, the X-ray diffraction powder pattern has been indexed assuming a hexagonal unit cell, which possibly includes rings of edge-sharing $Al(OH)_6$ octahedra.[24] The presence of octahedrally coordinated Al for CAH_{10} has previously been confirmed from a ^{27}Al MAS NMR spectrum recorded at 6.3 T and ν_r = 2.7 kHz by Gessner et al.[32] The center of gravity for the centerband was observed at 3 ppm[32] and from the reported spectrum the line width of the centerband is estimated to be fwhm ≈ 44 ppm.

C_3AH_6. The initially formed hydrates (CAH_{10} and C_2AH_8), resulting from the hydration of *HAC*, are metastable and tend to convert into the thermodynamically stable hydrate C_3AH_6. The 9.4-T ^{27}Al MAS NMR spectra of C_3AH_6 and a partially

(32) Gessner, W.; Müller, D.; Behrens, H.-J.; Scheler, G. *Z. Anorg. Allg. Chem.* **1982**, *486*, 193.

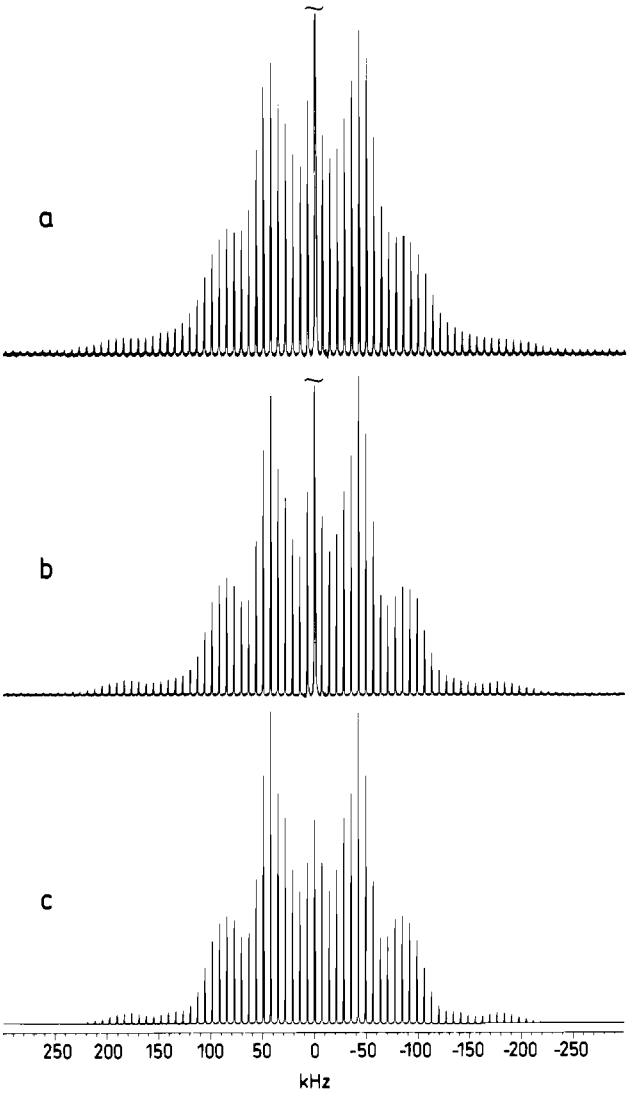

Figure 8. ^{27}Al (104.2 MHz) MAS NMR spectra illustrating the satellite transitions for (a) C_3AH_6 and (b) a partially deuterated sample $C_3A(D,H)_6$. The experimental spectra, recorded using $\tau_p = 1$ μs, $\gamma H_1/2\pi \approx 40$ kHz, ^1H decoupling, and $\nu_r = 7050$ Hz, are displayed with the central transition cut-off at 1/7 of its total height. (c) Simulated spectrum of the satellite transitions obtained using the above parameters and $C_Q = 0.705$ MHz and $\eta = 0.09$, as determined from least-squares fitting of the ssb intensities in part b. The simulation used Gaussian line widths of 300 and 400 Hz for the $(\pm^1/_2, \pm^3/_2)$ and $(\pm^3/_2, \pm^5/_2)$ satellite transitions, respectively.

deuterated sample ($C_3A(H,D)_6$), obtained with ^1H decoupling and identical spinning speeds ($\nu_r = 7050$ Hz), are shown in Figure 8a,b. Almost identical linewidths for the centerbands and ssb's are observed for the two samples. Comparison of the shape for the manifolds of ssb's for C_3AH_6 and $C_3A(H,D)_6$ shows that the ssb envelope for C_3AH_6 appears to be slightly smeared out. This is most clearly observed in the regions for the singularities of the outer satellite transitions (i.e., at ca. ±60 to ±80 kHz). The difference in ssb envelope for the two samples is most likely caused by minor variations in the quadrupole couplings for some of the AlO_6 octahedra within the C_3AH_6 sample, probably reflecting a lower degree of crystallinity compared to $C_3A(H,D)_6$. The observed ssb manifolds from the satellite transitions for these samples display characteristic first-order quadrupolar ssb patterns for an Al site with nearly axially symmetric electric field gradients. Optimization of simulated to experimental ssb intensities for $C_3A(H,D)_6$ (Figure 8b) results in the optimum simulated spectrum in Figure 8c, which corresponds to $C_Q = 0.705 \pm 0.010$ MHz and $\eta = 0.09 \pm 0.02$. The high accuracy of C_Q and η has been verified from simulations of five additional experimental ^{27}Al MAS spectra employing spinning speeds from 3.8 to 9.4 kHz. All optimum fitted spectra lead to quadrupolar coupling parameters within the uncertainty limits quoted above for C_Q and η. From the ^{27}Al MAS spectra of the two samples in Figure 8 an isotropic chemical shift of $\delta = 12.36 \pm 0.06$ ppm is obtained in both cases. Our results are therefore in agreement with the reported cubic crystal structure,[33] in which the unit cell contains a single octahedrally coordinated Al site. A static ^{27}Al NMR spectrum of C_3AH_6 has been reported earlier,[34] and from this spectrum one is able to estimate $C_Q \approx 0.77$ MHz. In a preliminary report on determination of C_Q and η from ssb's from ssb's for the satellite transitions,[17] $C_Q = 0.688$ MHz and $\eta = 0.00$ were obtained for $C_3A(H,D)_6$. These values deviate slightly from those in reported here, which may be due to the application of ^1H decoupling and to the use of improved versions of our simulation software[10] in the present study. ^1H decoupling has a marked effect on the linewidths of the centerband as well as the ssb's. This is illustrated by ^{27}Al MAS ($\nu_r = 3.8$ kHz) NMR spectra of C_3AH_6, where the observed line widths (fwhm) decreases from 1200 to 250 Hz for the centerband and from 800 to 250 Hz for the ssb's, when ^1H decoupling is applied.

γ-AH_3. Hydration of *HAC* also leads to the formation of amorphous alumina gel (AH_n), which gradually crystallizes into gibbsite (γ-AH_3). ^{27}Al MAS NMR spectra of synthetic γ-AH_3, recorded at 7.1 and 9.4 T, are shown in Figure 9. Figure 9a illustrates the relative intensities for the central and satellite transitions observed over a spectral width of 2 MHz at 9.4 T, while the expansions in Figure 9d,b show experimental spectra for the centerbands of the central transitions at 7.1 and 9.4 T, respectively. From the spectra of the central transitions it is apparent that γ-AH_3 contains two nonequivalent Al atoms in octahedral environments, in agreement with the crystal structure determined by X-ray diffraction.[35] At 7.1 T the two central transitions overlap (Figure 9d) and display a quite narrow and featureless resonance at ca. 5 ppm for one of the Al sites, whereas some of the singularities, shoulders, and edges of a second-order line shape are observed for the other Al site, indicating a larger quadrupolar coupling for this site. At 9.4 T the resolution of the spectrum for the two central transitions decreases (Figure 9b) thus reducing the accuracy of any determination of C_Q and η for the two Al sites from analysis/simulation of the central transitions. However, examination of the ssb manifold from the satellite transitions, observed over a spectral range of ca. 1.5 MHz (Figure 9f), shows a well-defined shape for the overall ssb envelope, which is composed of overlapping ssb's from both Al sites. Quadrupole coupling parameters for the two Al sites in γ-AH_3 may therefore be determined from simulations of the experimental ssb envelope with ssb intensities for the two Al sites. When a 1:1 intensity ratio is employed for these sites, a four-parameter least-squares optimization of simulated to experimental ssb intensities give the following parameters for the ^{27}Al quadrupolar interactions in γ-AH_3. Al(1): $C_Q = 1.97 \pm 0.07$ MHz, $\eta = 0.73 \pm 0.04$. Al(2): $C_Q = 4.45 \pm 0.05$ MHz, $\eta = 0.44 \pm 0.03$. The optimum simulated spectrum for the satellite transitions is shown in Figure 9g, while Figure 9 parts i and h displays the individually simulated ssb patterns for Al(1) and Al(2), respectively. A convincing agreement between experimental and simulated spectra for the satellite transitions (Figure 9f,g) is observed. Finally, the C_Q and η values resulting from the four-parameter fit of the satellite transitions have been used in simulations of the line shape for the central transitions; excellent agreement is obtained with the experimental spectra, as shown by the simulated centerbands in Figure 9c,e at the two applied magnetic fields. From these simulations chemical shifts of $\delta = 10.4 \pm 0.3$ ppm for Al(1) and

(33) Cohen-Addad, C.; Ducros, P.; Bertaut, E. F. *Acta Crystallogr.* **1967**, *23*, 220.
(34) Lahajnar, G.; Blinc, R.; Rutar, V.; Smolej, V.; Zupancic, I.; Kocuvan, I.; Ursic, J. *Cem. Concr. Res.* **1977**, *7*, 385.
(35) Saalfeld, H.; Wedde, M. *Z. Kristallogr.* **1974**, *139*, 129.

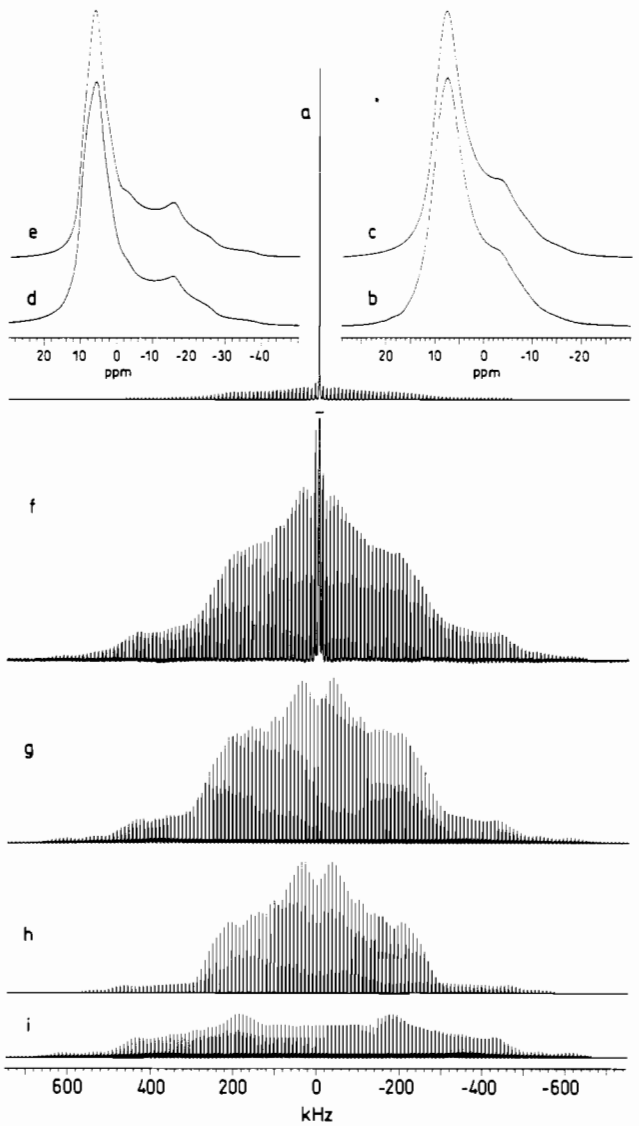

Figure 9. ^{27}Al MAS NMR spectra of γ-AH_3 obtained at (d) 7.1 T and (a, b, f) 9.4 T using τ_p = 1 μs, $\gamma H_1/2\pi \approx 40$ kHz, ^{1}H decoupling, and spinning speeds of 8.0 kHz and 9.25 kHz, respectively. Part a illustrates the relative intensities of the central and satellite transitions at 9.4 T, while the vertical expansion in part f displays the ssb envelope for the satellite transitions. (g) Optimum simulated spectrum of the ssb's for the two overlapping Al sites employing the parameters above and C_Q = 1.97 MHz, η = 0.73 for Al(1) and C_Q = 4.45 MHz, η = 0.44 for Al(2), and a 1:1 intensity ratio for the two Al sites. Simulated spectra of the individual Al sites are shown in part h for Al(1) and (i) for Al(2). The simulated spectra employed Gaussian line widths of 600 and 1200 Hz for Al(1) and 1000 and 2500 Hz for Al(2), for the ($\pm^1/_2$, $\pm^3/_2$) and ($\pm^3/_2$, $\pm^5/_2$) satellite transitions, respectively. Simulated centerbands for the central transitions at 7.1 and 9.4 T, using the same C_Q, η values and intensity ratio as in part g, are shown in parts e and c, respectively.

δ = 11.5 ± 0.3 ppm for Al(2) are determined. The ^{27}Al MAS NMR spectrum (6.3 T) of the central transitions for synthetic γ-AH_3 has recently been studied by Woessner,[8] and C_Q, η, and δ values for the two Al sites (Al(1), C_Q = 2.0 MHz, η = 0.8, δ = 11.0 ppm; Al(2), C_Q = 4.30 MHz, η = 0.40, δ 9.0 ppm) were reported from line-shape simulations of the centerbands. These values agree favorably with those obtained from simulations of the ssb intensities in this investigation. However, for the simulated spectra Woessner[8] used a relative intensity ratio of 58:42 for the Al(1) and Al(2) sites, in contrast to the ratio of 1:1 employed for the spectra in this study.

Aluminate Phases in Portland Cements. Tricalcium aluminate (C_3A) and calcium aluminoferrite (C_4AF) are the main aluminate phases in Portland cement. They are usually present in the 1–15% (w) range, with C_3A as the most important phase in ordinary Portland cement. Hydration of C_3A in the presence of gypsum (e.g., as in Portland cements, Figure 1b) initially produces the sulfate-containing phase, ettringite ($C_6A\bar{S}_3H_{32}$), which slowly converts to the thermodynamically stable monosulfate ($C_4A\bar{S}H_{12}$).[25] The course of the hydration of the aluminate phases can have a considerable influence on the physical and chemical properties of hardened Portland cement. For instance, the formation of ettringite can affect the early workability and setting behavior, and in the long term, the durability can also be affected by the nature of the calcium aluminates and their hydration behavior.

C_3A. Using ^{27}Al MAS NMR spectra of C_3A at 7.1 T and 9.4 T as an example, we have recently demonstrated the potential of high-speed spinning (ν_r = 18–20 kHz) for determination of strong quadrupolar interactions from MAS NMR spectra of the central transition.[9] In agreement with the crystal structure of C_3A,[36] these spectra display overlapping central transitions from the two tetrahedrally coordinated Al sites. Quadrupole coupling and chemical shift parameters for the two Al sites, determined from line-shape simulations of the centerband spectrum recorded at 9.4 T in our earlier work,[9] are listed in Table I. To confirm the C_Q, η, and δ values and thereby the assignment of the spectrum reported for C_3A, a comparison of the experimental and simulated spectra obtained at 7.1 T (ν_r = 18.7 kHz) and 11.7 T (ν_r = 14.8 kHz) is shown in Figure 10. The simulated spectra in Figure 10a,c are generated using the parameters listed in Table I and include the central transition, the ($\pm^1/_2$, $\pm^3/_2$) satellite transitions, and their ssb's. Figure 10 illustrates that at 11.7 T the widths of the two overlapping centerband line shapes are considerably reduced as compared to those in the spectrum at 7.1 T. For example, at 11.7 T the low-intensity shoulder at lowest frequency ends at ca. –5 ppm, whereas at 7.1 T the shoulder stretches out to ca. –110 ppm. Thus, completely undistorted centerbands are observed for $\nu_r \gtrsim 13$ kHz at 11.7 T, while $\nu_r \gtrsim 19$ kHz is required at 7.1 T. C_3A has also been studied by static and MAS ($\nu_r \approx$ 7 kHz) NMR at 11.7 T.[12] However, these spectra were analyzed in terms of only one set of C_Q, η, and δ parameters (C_Q = 9.7 MHz, η = 0.3, and δ = 85 ppm),[12] a result that probably should be attributed to the observed highly distorted MAS spectrum caused by the use of too low a spinning speed.

$C_6A\bar{S}_3H_{32}$. Experimental ^{1}H decoupled ^{27}Al MAS NMR spectra of ettringite ($C_6A\bar{S}_3H_{32}$), the initial hydration product of the calcium aluminates in Portland cements, recorded at 9.4 T and with spinning speeds of 2.7 and 7.3 kHz are shown in parts a and b of Figure 11, respectively. These spectra display characteristic features for a single ^{27}Al resonance with a small quadrupole interaction, i.e., a narrow line width for the central transition (fwhm = 100 Hz) and a complete manifold of ssb's for the satellite transitions extending over a spectral range of ca. 250 kHz. Determination of the quadrupole coupling parameters from least-squares fitting of simulated to experimental ssb intensities requires an initial set of C_Q and η values as input to the optimization routine. A good estimate of C_Q and η may be obtained from the *SOQE* parameter in combination with the numerical frequency for the inner singularities ($|\nu_i|$) of the ($\pm^1/_2$, $\pm^3/_2$) transitions, as described recently.[10] Alternatively, the ^{27}Al MAS NMR spectra of ettringite appears to be a suitable example for illustrating the determination of *SOQE* from moment analysis (vide supra), in the instance of very weak quadrupole interactions (i.e., $C_Q \lesssim 0.5$ MHz for $I = {}^5/_2$). Employing eqs 1–4 and using the integrated intensities of the centerband and ssb's for the spectrum in Figure 11b, the moment analysis gives *SOQE* = 0.37 ± 0.01 MHz for ettringite. By the usual method *SOQE* is determined from the difference in second-order quadrupolar shifts of the central and ($\pm^3/_2$, $\pm^1/_2$) transitions,[17,18] i.e., $(\delta^{c.g.}_{\pm 3/2,\pm 1/2} - \delta^{c.g.}_{1/2,-1/2}) = 27SOQE^2/(4000\nu_L)$ for I = 5/2. For *SOQE* = 0.37 MHz, this

(36) Mondal, P.; Jeffrey, J. W. *Acta Crystallogr.* **1975**, *B31*, 689.

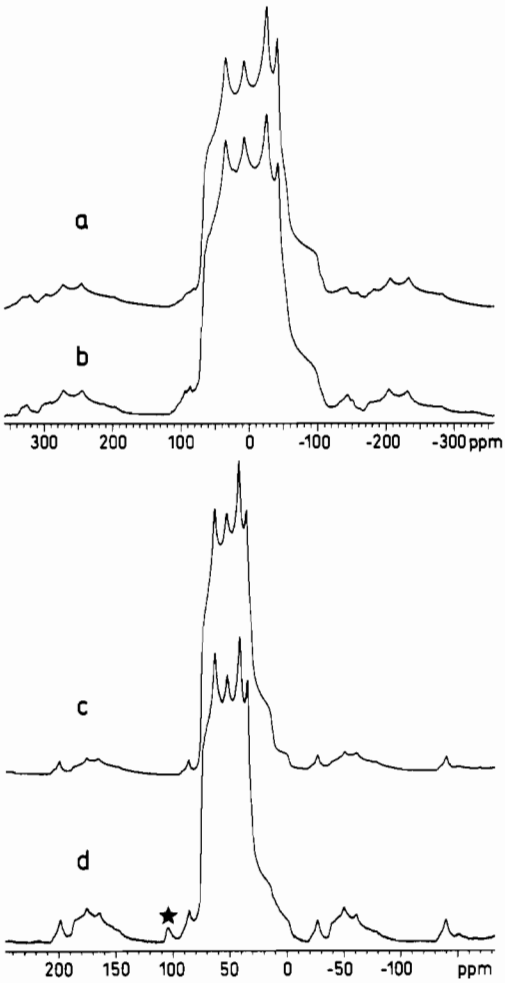

Figure 10. ^{27}Al MAS NMR spectra of C_3A recorded at (b) 7.1 and (d) 11.7 T, employing spinning speeds of 18.7 and 14.8 kHz, respectively. Simulated spectra at (a) 7.1 and (c) 11.7 T, including the central transition and the ($\pm^1/_2, \pm^3/_2$) satellite transitions. The simulations employed the C_Q, η, and δ values listed in Table I for the two Al sites in C_3A. Simulations of the ssb's in part d indicate that the 11.7-T spectrum is recorded slightly off the magic angle (θ = 54.74°). The best agreement between experimental and simulated ssb's is observed for θ = 54.80°, which is employed for the simulated spectrum in part c. The asterisk indicate an Al impurity (Al–N) from the Si_3N_4 rotor material.

corresponds to $(\delta^{c.g.}_{\pm 3/2,\pm 1/2} - \delta^{c.g.}_{1/2,-1/2})$ = 8.9 Hz, which most probably cannot be determined experimentally if the line widths of the central transition (100 Hz) and ssb's (ca. 200 Hz) are taken into account. However, for larger quadrupolar couplings ($C_Q \approx$ 1–3 MHz) *SOQE* is expected to be obtained with higher accuracy from the $(\delta^{c.g.}_{\pm 3/2,\pm 1/2} - \delta^{c.g.}_{1/2,-1/2})$ shift-difference, since the moment analysis leading to eqs 1–4 assumes ideal conditions for the excitation/detection. Employing *SOQE* = 0.37 MHz as determined from moment analysis and the estimated value $|\nu_l|$ = 21 kHz from Figure 11a gives C_Q = 0.367 MHz and η = 0.24 for ettringite following the procedure described above and elsewhere.[10] Refinements of these values is performed by least-squares fitting to the ssb's in Figure 11a, which contains a large number of ssb's available for the optimization routine and thereby improves the definition of the ssb envelope, compared to the spectrum obtained using the higher spinning speed (Figure 11b). This refinement gives C_Q = 0.360 ± 0.010 MHz and η = 0.19 ± 0.03, and the corresponding simulated spectra for the two applied spinning speeds are shown in Figure 11c,d. Minor deviations between experimental and simulated ssb intensities are ascribed to a small dispersion in the quadrupole coupling parameters for the actual sample of ettringite (e.g., similar to the observation for the C_3AH_6 sample in Figure 8a). For both spectra in Figure 11 an isotropic chemical shift of δ = 13.10 ● 0.10 ppm is obtained.

The experimental spectra as well as the single set of C_Q, η, and δ values demonstrates that all Al nuclei are in equivalent, octahedrally coordinated positions in the unit cell of ettringite. This disagrees with the proposed crystal structure by Moore and Taylor,[37] who reported two nonequivalent Al sites in the unit cell from single-crystal X-ray diffraction. According to Moore and Taylor[37] the crystal structure for ettringite consists of columns of composition $\{Ca_6Al_2(OH)_{12}\cdot 24H_2O\}^{6+}$ arranged parallel to the c axis as illustrated in Figure 12. The channels between the columns are occupied by SO_4^{2-} anions and water molecules and has the composition $\{3SO_4\cdot 2H_2O\}^{6-}$. In their proposed structure equal Al–O bond lengths are reported for one of the AlO_6 octahedra (Al(1), d_{Al-O} = 1.92 Å (×6)), while the other Al site contains two different Al–O distances (Al(2), d_{Al-O} = 1.82 Å (×3) and d_{Al-O} = 2.00 Å (×3))[37] (see Figure 12). Obviously, such variations in the geometries of the AlO_6 octahedra should result in two distinct sets of C_Q, η, and δ parameters, which disagree with the ^{27}Al MAS NMR spectra of ettringite in Figure 11.

$C_4A\bar{S}H_{12}$. Monosulfate ($C_4A\bar{S}H_{12}$) is typically formed by conversion of the higher sulfate containing ettringite phase during the continued hydration of C_3A in Portland cements. The ^{1}H-decoupled ^{27}Al MAS NMR spectrum of a synthetic sample of monosulfate at 9.4 T using ν_r = 7.2 kHz (Figure 13a,b) displays a single resonance (fwhm = 300 Hz) for the central transition in the region for octahedrally coordinated Al. This is in accord with the reported XRD crystal structure for monosulfate.[38] The difference in quadrupolar shift between the central and the ($\pm^1/_2, \pm^3/_2$) satellite transitions gives *SOQE* = 1.7 ± 0.2 MHz and thus 1.3 MHz ≤ C_Q ≤ 1.9 MHz. Using the *SOQE* value an isotropic ^{27}Al chemical shift δ = 11.8 ± 0.2 ppm is obtained. The values for both *SOQE* and δ were confirmed by the ^{27}Al MAS NMR spectrum obtained at 7.1 T. The "bell-shaped" envelope for the ssb's of the satellite transitions extends over a spectral range of ca. 0.9 MHz (Figure 13a) and shows no direct resemblance to simulated ssb patterns for a *single* set of C_Q, η values. Therefore, the "bell-shaped" ssb pattern most probably results from a distribution of quadrupole coupling parameters within the monosulfate sample. Indeed, the simulated ssb envelope shown in Figure 13c, obtained by addition of 10 simulated ssb patterns with slightly different C_Q and η values, supports this supposition. The individual simulations, constituting the overall ssb spectrum in Figure 13c, employ quadrupole coupling parameters in the range 1.3 MHz ≤ C_Q ≤ 1.7 MHz and 0.3 ≤ η ≤ 1.0. Figure 13c agrees quite satisfactorily with the experimentally observed ssb manifold for monosulfate (Figure 13a), thereby illustrating that the "bell-shaped" ssb envelope may be simulated using only 10 overlapping ssb patterns with a restricted distribution in the C_Q and η values. We note that ssb envelopes with similar appearance have recently been reported from ^{27}Al MAS NMR spectra of some aluminosilicate sodalites.[39] The distribution in C_Q and η may reflect crystal defects, disorder, and/or dynamic processes (OH exchange) within the sample.

C_4AH_{13}. In the absence of calcium sulfate in Portland cement, C_3A can react with calcium hydroxide and water to form the hydrate C_4AH_{13}. This reaction may occur in Portland cements with a low SO_3/Al_2O_3 ratio, where the small amount of SO_3 is consumed during the initial formation of ettringite (Figure 1). With the excess of calcium hydroxide formed by the hydration of the silicate phases, further hydration of C_3A can produce C_4AH_{13}, which occurs either as a solid solution with monosulfate or as a discrete phase.[25] The ^{1}H-decoupled ^{27}Al MAS NMR

(37) Moore, A. E.; Taylor, H. F. W. *Acta Crystallogr.* **1970**, *B26*, 386.
(38) Allmann, R. *Neues Jahrb. Mineral. Monatsh.* **1977**, 136.
(39) Nielsen, N. C.; Bildsøe, H.; Jakobsen, H. J.; Norby, P. *Zeolites* **1991**, *11*, 622.

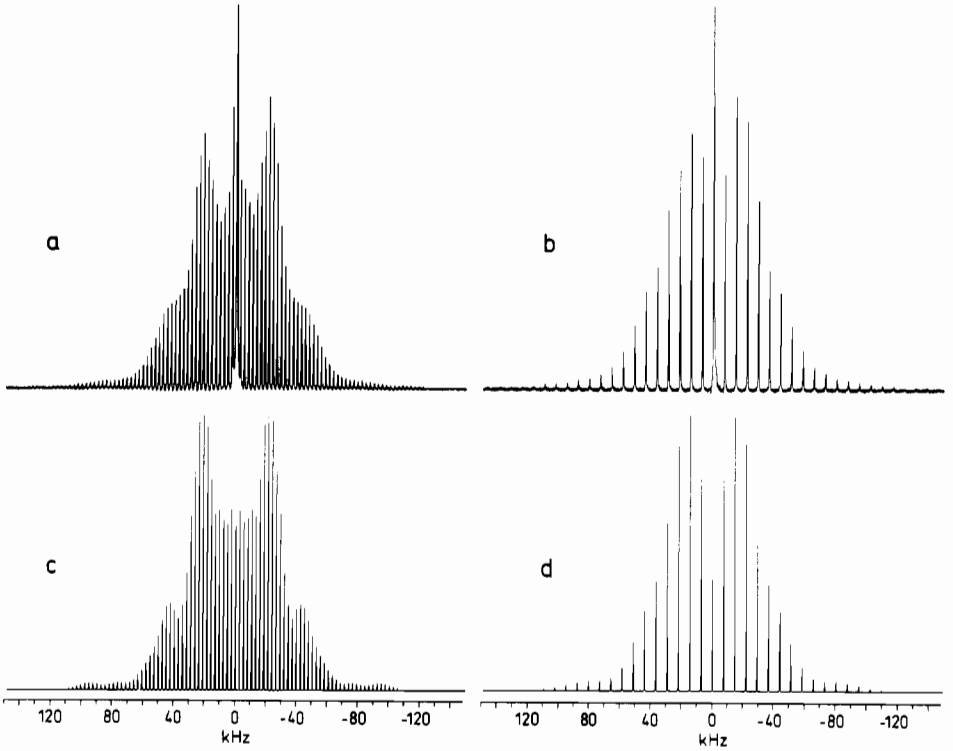

Figure 11. ^{27}Al MAS NMR spectra of ettringite ($C_6A\bar{S}_3H_{32}$) obtained at 9.4 T using τ_p = 2 μs, $\gamma H_1/2\pi \approx 40$ kHz, and spinning speeds of (a) 2.7 and (b) 7.3 kHz. The central transition is cut off at $^1/_{14}$ and $^1/_7$ of its total height in parts a and b, respectively. Simulated spectra of the satellite transitions in parts a and b are shown in parts c and d. The simulations employed the τ_p, $\gamma H_1/2\pi$, and ν_r values given above and the computer-optimized quadrupole coupling parameters (C_Q = 0.360 MHz, η = 0.19). Gaussian line widths of 200 and 400 Hz for the ($\pm^1/_2$, $\pm^3/_2$) and ($\pm^3/_2$, $\pm^5/_2$) satellite transitions were used in the simulated spectra.

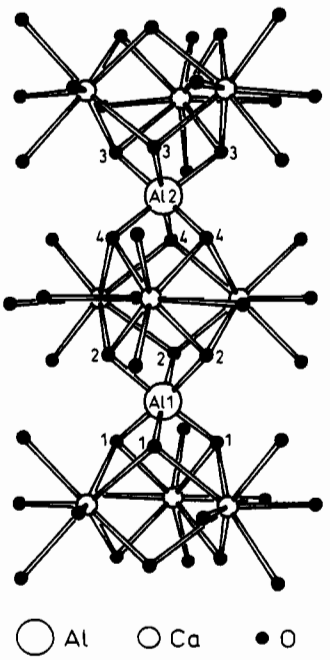

Figure 12. ORTEP diagram of part of a single column in ettringite with composition $\{Ca_6Al_2(OH)_{12}\cdot 24H_2O\}^{6+}$, obtained using the atomic coordinates and crystal data (trigonal with space group $P31c$) reported by Moore and Taylor.[37] Each of the columns in the unit cell are parallel to the c axis. For simplicity the hydrogen atoms are not included in the diagram. The indices of the oxygen atoms, constituting the first coordination sphere around Al(1) and Al(2), are shown and the corresponding bond lengths[37] are $d_{Al1\text{-}O1}$ = 1.92 Å, $d_{Al1\text{-}O2}$ = 1.92 Å, $d_{Al2\ O3}$ = 2.00 Å, and $d_{Al2\text{-}O4}$ = 1.82 Å.

spectrum of a synthetic sample of C_4AH_{13}, recorded at 9.4 T using ν_r = 7.2 kHz, is shown in Figure 13d,e. From the spectrum of the central transition (Figure 13e) it is apparent that C_4AH_{13} contains a single Al site in an octahedral environment, in agreement with the XRD crystal structure.[40] The difference in quadrupolar shift between the central and ($\pm^1/_2$, $\pm^3/_2$) satellite transitions gives *SOQE* = 1.8 ± 0.2 MHz, and using this value an isotropic chemical shift of δ = 10.2 ± 0.2 ppm is determined. An ^{27}Al MAS NMR spectrum obtained at 7.1 T confirms the values for both *SOQE* and δ. Examination of the ssb manifold from the satellite transitions, observed over a spectral range of ca. 0.9 MHz (Figure 13d), shows an overall ssb envelope with some characteristic features for a ssb pattern with an asymmetry parameter in the range of ca. 0.6–0.9. However, the ssb pattern appears somewhat smeared out and cannot be simulated with a single set of C_Q, η values. Addition of 10 simulated ssb spectra, with slightly different quadrupole coupling parameters (1.5 MHz $\leq C_Q \leq$ 2.2 MHz and $0.6 \leq \eta \leq 0.85$), produces an overall ssb envelope (Figure 13f) which is in reasonably good agreement with the experimentally observed ssb manifold for C_4AH_{13}. The slight variation in the ^{27}Al quadrupole coupling parameters may reflect the observation from the XRD study,[40] that the interlayer region between the basic octahedral layers of composition $Ca_2Al(OH)_6$ is only partly ordered, with H_2O molecules distributed among a number of sites. However, comparison of the experimental ssb envelopes for monosulfate (Figure 13a) and C_4AH_{13} (Figure 13d) indicates a higher degree of local order for the C_4AH_{13} sample.

Hydrated Cements. High Alumina Cement. The initial hydration of the calcium aluminates in *HAC* and Portland cements is accompanied by conversion of the Al coordination state from Al(4) to Al(6). As previously demonstrated,[5,11,13,14] this allows the hydration processes to be easily followed by ^{27}Al MAS NMR, i.e., by a decrease of the ^{27}Al chemical shift from ca. 70–80 ppm to 5–15 ppm during the conversion of Al(4) to Al(6). However, identification of the individual Al phases in complex systems such as "real" cements could prove to be quite difficult using solely the ^{27}Al chemical shifts determined for the synthetic phases, because of the very limited variation in δ values within the regions

(40) Ahmed, S. J.; Taylor, H. F. W. *Nature* **1967**, *215*, 622.

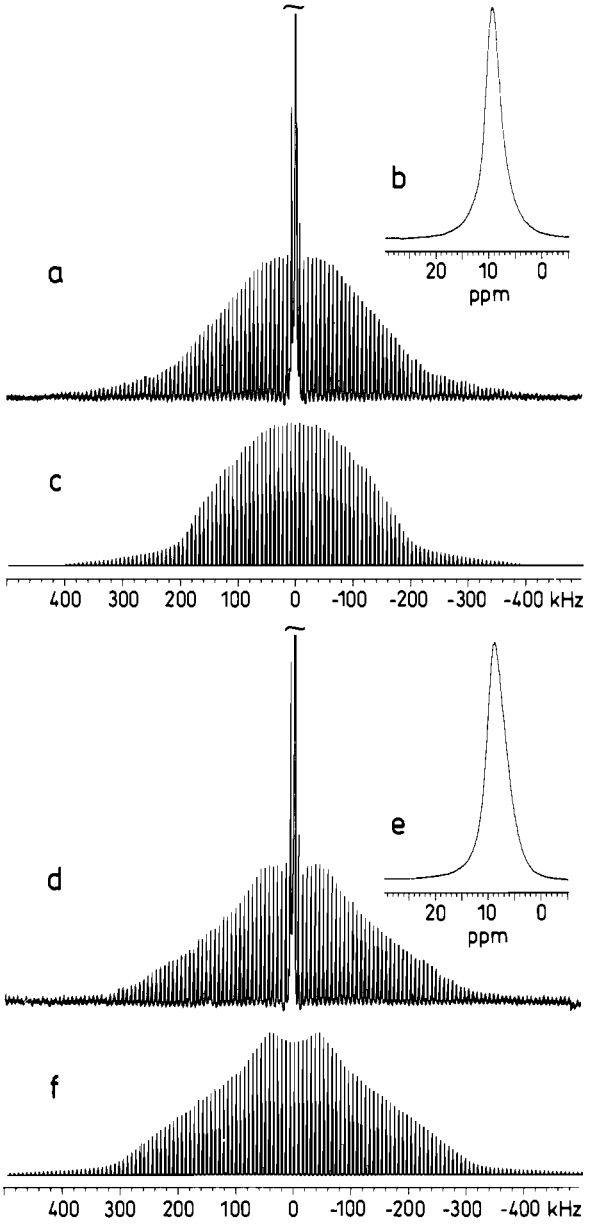

Figure 13. ^{27}Al MAS NMR spectra of (a) monosulfate ($C_4A\bar{S}H_{12}$) and (d) C_4AH_{13} obtained with ^{1}H decoupling. $\tau_p = 1$ μs, $\gamma H_1/2\pi \approx 40$ kHz, and $\nu_r = 7.2$ kHz for both spectra. The central transition is cut off at $^1/_{19}$ of its total height in part a and the spectrum illustrates a "bell-shaped" envelope of ssb's from the satellite transitions. (b) Expansion of the central transition for monosulfate, which has a natural line width of 300 Hz. (c) Simulation of the ssb envelope for monosulfate obtained by addition of 10 simulated ssb patterns with quadrupole coupling parameters in the range 1.3 MHz $\leq C_Q \leq$ 1.7 MHz and $0.3 \leq \eta \leq 1.0$. (d) Vertical expansion by a factor of 24 of the ssb's from the satellite transitions in C_4AH_{13}. (e) Expansion of the central transition for C_4AH_{13} (fwhm = 400 Hz). (f) Simulation of the ssb manifold in part d obtained by addition of 10 ssb patterns with slightly different C_Q, η values (1.5 MHz $\leq C_Q \leq$ 2.2 MHz and $0.6 \leq \eta \leq 0.85$). The simulations in parts c and f employed Gaussian linewidths of 900 and 1200 Hz for the ($\pm^1/_2$, $\pm^3/_2$) and ($\pm^3/_2$, $\pm^5/_2$) satellite transitions, respectively.

for Al(4) and Al(6) (e.g., see Table I). The previous sections have demonstrated that considerably larger variations are observed for the ^{27}Al quadrupole coupling parameters of the synthetic calcium aluminates and calcium aluminate hydrates. In ^{27}Al MAS NMR this variation in C_Q and η values provides characteristic line shapes and/or ssb manifolds for different Al sites, which can facilitate identification of the individual Al components. As an illustrative example, the ^{27}Al MAS NMR spectrum of a hydrated *HAC* (Alcoa CA-14), hydrated for 28 days using a water/cement ratio of 0.4 and recorded at 9.4 T employing ν_r =

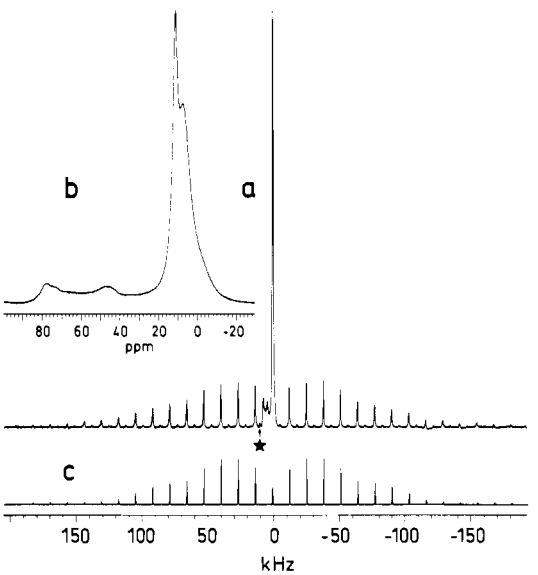

Figure 14. ^{27}Al MAS NMR spectra of a hydrated high alumina cement (Alcoa CA-14, hydrated for 28 days) recorded at 9.4 T employing ^{1}H decoupling. $\tau_p = 2$ μs, $\gamma H_1/2\pi \approx 40$ kHz, and $\nu_r = 13.1$ kHz. (a) Illustration of the total height of the central transitions and the ssb manifolds from the satellite transitions. (b) Expansion of the spectral region for the central transitions. (c) Simulation of the ssb pattern observed in part a using the quadrupole coupling parameters of C_3AH_6 (see Table I). The asterisk in part a indicates an Al impurity (Al–N) from the Si_3N_4 rotor.

13.1 kHz (Figure 14), allows identification of four different Al phases in this sample. CA and CA_2 constitute the main aluminate phases in *HAC*, and the hydration chemistry for these phases is illustrated in Figure 1a. Two components with Al in octahedral environments are observed from the partly overlapping centerbands at 8 and 12 ppm (Figure 14b), where the Al site with the centerband resonance at 12 ppm displays intense ssb's from the satellite transitions. The observed ssb manifold from this site is in excellent agreement with the quadrupole coupling parameters determined for C_3AH_6 (Table I), as demonstrated by the simulated ssb spectrum in Figure 14c using these parameters. The partly overlapping resonance at 8 ppm corresponds to the position for the central transition for the Al(1) site in γ-AH_3 (Figure 9), when the additional line broadening of the centerband observed in the spectrum of *HAC* (Figure 14) is taken into account. The Al(2) site from γ-AH_3 (i.e., the Al site with largest quadrupole coupling) is observed as an unresolved shoulder at a lower chemical shift. The absence of ssb's from the AH_3 phase indicates that AH_3 in the hydrated *HAC* sample is not present in a crystalline form (as observed for γ-AH_3, Figure 9) but most likely as AH_3 gel. This may also explain the additional line broadening of the centerband resonances in hydrated *HAC* compared to that of γ-AH_3 in Figure 9. In the Al(4) chemical shift range of Figure 14b two broadened resonances are observed at ca. 78 and 45 ppm. These originate from minor amounts of unhydrated calcium aluminates in the *HAC* sample. From a comparison of these positions with the ^{27}Al MAS NMR spectra in Figures 2 and 5, it is apparent that the peak at 78 ppm corresponds to the overlapping resonances from the six Al sites in CA, while the peak at 45 ppm corresponds to the singularities of the centerband line shape for the Al site with smallest quadrupole coupling in CA_2. The Al(4)/Al(6) intensity ratio for the hydrated HAC sample reflects the quantities of unhydrated/hydrated aluminate phases and from integration of the spectral regions for Al(4) and Al(6) in Figure 14b, a rough estimate of the Al(4)/Al(6) atomic ratio of 0.14 ± 0.01 is obtained. Improved accuracy of the Al(4)/Al(6) atomic ratio, as well as quantification of the individual Al components in the *HAC* sample, may be accomplished by computer deconvolutions of all central transition centerbands in

the ^{27}Al MAS NMR spectrum. Deconvolution of the partly overlapping centerbands in the Al(6) region in Figure 14b, employing second-order quadrupolar line shapes for the Al site in C_3AH_6 and the two Al sites in AH_3, gives an C_3AH_6/AH_3 intensity ratio of 0.30 ± 0.02, corresponding to a weight ratio of 0.72 ± 0.05 for C_3AH_6/AH_3. We note that for hydrated *HAC* samples with higher molar Al(4)/Al(6) ratios, it is a necessity that such deconvolutions should also include second-order quadrupolar line shapes for each Al(4) and Al(6) component, because some centerband line shapes extend over the chemical shift ranges for Al(4) as well as Al(6) (e.g., CA_2). In quantitative ^{27}Al MAS NMR it is also necessary to take account of effects from the different excitation profiles of the individual Al components. In the ^{27}Al MAS NMR experiment on *HAC* hydrated for 28 days, a strong *xy* field strength ($\gamma H_1/2\pi$) and a short pulse width (τ_p) were used in order to fulfill the condition $(I + {}^1/_2)(\gamma H_1/2\pi)\tau_p \leq {}^1/_{12}$, which ensures observation of reliable signal intensities from Al sites with different quadrupolar couplings.[41]

Portland Cement. Despite the low Al content of Portland cement, the hydration processes of the calcium aluminate phases can have an important impact on the properties of hardened Portland cement, and thus identification/quantification of such phases are of general interest in cement chemistry. In ordinary Portland cements C_3A constitutes the main aluminate phase and the hydration reactions for C_3A in the presence and absence of gypsum are illustrated in parts b and c of Figure 1, respectively. ^{27}Al MAS NMR spectra of an ordinary Portland cement (Cementa AB, Sweden) hydrated for 1 and 28 days, recorded at 9.4 and 7.1 T, respectively, are shown in Figure 15. These illustrate that detailed information about the calcium aluminate hydrates in Portland cement can be obtained from ^{27}Al MAS NMR spectroscopy. After hydration for 1 day, the centerband region of the ^{27}Al MAS (ν_r = 3.7 kHz) NMR spectrum (Figure 15b) displays a narrow resonance at 13 ppm, with a weak shoulder at ca. 5 ppm and ssb's over a spectral range of ca. 200 kHz. The narrow centerband at 13 ppm is in agreement with the chemical shift of ettringite, while the shoulder at lower chemical shift is assigned to minor amounts of monosulfate and/or C_4AH_{13}. The broad centerband resonance from ca. 80 ppm to 40 ppm (which overlap with two ssb's at 48 and 84 ppm from ettringite) is ascribed to unhydrated material in the Portland cement. In contrast to the characteristic ssb pattern observed for the single Al site in synthetic ettringite (Figure 11), the ssb's from ettringite in Portland cement display a rather featureless ssb envelope. A simulated ssb manifold (Figure 15c), with a similar appearance as observed in Figure 15a, is obtained by the addition of nine ssb patterns with slightly different quadrupole coupling parameters in the range 0.25 MHz ≤ C_Q ≤ 0.40 MHz and 0.19 ≤ η ≤ 1.00. Comparison of this simulated ssb manifold with the ssb pattern in Figure 15d, which corresponds to the single set of C_Q and η values determined for synthetic ettringite, suggests that the ssb manifold observed for ettringite in Portland cement reflects a distribution of C_Q and η values. Thus, ettringite is not present in a highly crystalline form in Portland cement, consistent with the probability that "impurity" ions such as Fe^{3+}, Si^{4+}, Mg^{2+}, and K^+ are incorporated in the lattice.

After hydration for 28 days, the ^{27}Al MAS NMR spectrum of the Portland cement sample, obtained at 7.1 T with ν_r = 8.1 kHz (Figure 15e,f), displays two partly overlapping centerbands at 13 and 8.5 ppm. A broad resonance from ca. 80 to 40 ppm is also observed which reflects the presence of some unhydrated material. The observed ssb's corresponding to the centerband at 13 ppm is assigned to ettringite, whilst the centerband at 9 ppm agrees well with the isotropic chemical shift of monosulfate, if the second-order quadrupolar shift is taken into account. The centerband from C_4AH_{13} has a center of gravity at 7.0 ppm at 7.1 T, and it cannot therefore be certain if the line-broadened resonance at 9 ppm, observed in Figure 15f, also includes the centerband from a minor amount of this hydrate. The relative amounts of ettringite and monosulfate in the actual sample of hydrated Portland cement may be determined by computer deconvolution of the partly overlapping centerbands. It is noted that observation of reliable signal intensities from the Al sites with different quadrupole couplings was ensured by the use of a strong rf field strength ($\gamma H_1/2\pi$) and a short pulse width (τ_p) (e.g., $(I + {}^1/_2)(\gamma H_1/2\pi)\tau_p \leq {}^1/_{12}$)[41] in the ^{27}Al MAS experiment. The deconvolution of the centerbands (Figure 15g) gives a monosulfate/ettringite intensity ratio of 3.3 ± 0.3 corresponding to a weight ratio of approximately 1.7 ± 0.2 for monosulfate/ettringite. The uncertainty limits are estimated from a visual comparison of slightly different computer deconvolutions of the experimental centerband. In contrast to the results from ^{27}Al MAS NMR, monosulfate could not be detected by X-ray diffraction in the Portland cement hydrated for 28 days, although

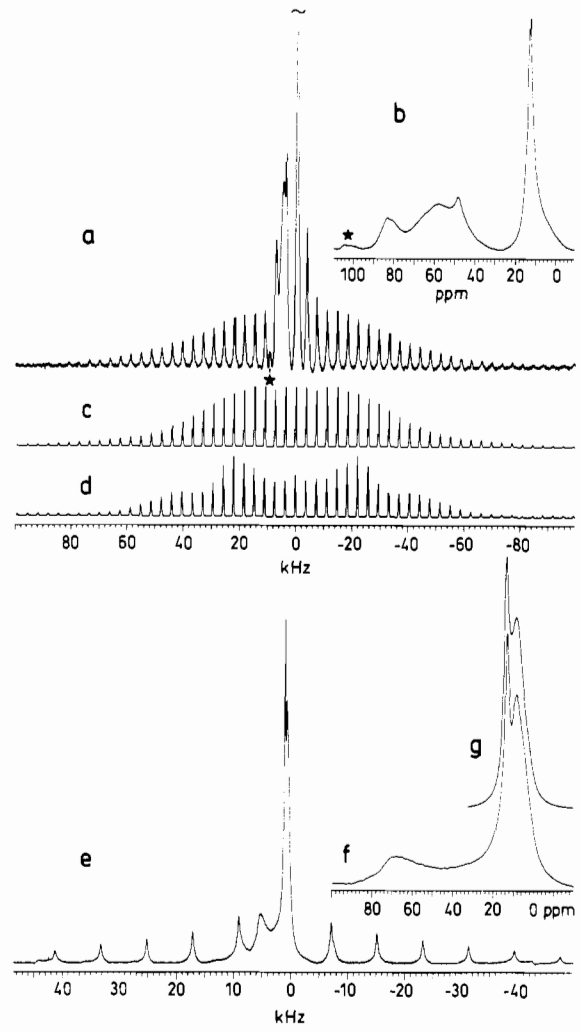

Figure 15. ^{27}Al MAS NMR spectra of an ordinary Portland cement hydrated for (a, b) 1 and (e, f) 28 days. (a) Experimental spectrum of the sample hydrated for one day obtained at 9.4 T using ^1H decoupling. τ_p = 2 μs, $\gamma H_1/2\pi \approx$ 40 kHz, and ν_r = 3.7 kHz. (b) Expansion of the central transitions in part a. (c) Simulation of the ssb manifold in part a obtained by addition of nine ssb spectra with C_Q, η values in the range 0.25 MHz ≤ C_Q ≤ 0.40 MHz and 0.19 ≤ η ≤ 1.00. (d) Simulation employing the quadrupole coupling parameters for ettringite (see Table I). (e) Experimental spectrum of the sample hydrated for 28 days, obtained at 7.1 T using ^1H decoupling, τ_p = 2 μs, $\gamma H_1/2\pi \approx$ 40 kHz, and ν_r = 8.1 kHz. Expansion of the central transitions in part e are shown in part f. (g) Deconvolusion of the centerbands for monosulfate and ettringite corresponding to an monosulfate/ettringite intensity ratio of 3.3 ± 0.3. The asterisks in parts a and b indicate an Al impurity (Al–N) from the Si_3N_4 rotor material.

(41) Samoson, A.; Lippmaa, E. *Phys. Rev. B.* **1983**, *28*, 6567.

Table II. Assignment of Quadrupole Coupling Parameters from the Mean Bond Angle Deviation (D) and a Calculated Estimate of the Geometrical Dependence of the EFG Tensor (V'_{zz}) for AlO_4 Tetrahedra in the Anhydrous Calcium Aluminates and Additional Compounds

compound	Al site[a]	C_Q[b] (MHz)	η[b]	D[c] (deg)	V'_{zz}[d] (10^{20} V m^{-2})	η'[d]	structure ref
CA_2	Al(1)	6.25	0.88	4.29	1.769	0.52	26
	Al(2)	9.55	0.82	5.07	2.051	0.81	
C_3A	Al(1)	8.69	0.32	5.18	1.987	0.90	36
	Al(2)	9.30	0.54	6.22	2.495	0.63	
$C_{12}A_7$	Al(1)	9.7	0.40	7.47	2.614	0.00	31
	Al(2)	3.8	0.70	3.16	1.307	0.00	
β-$LiAlO_2$		1.89[e]	0.56[e]	1.39	0.465	0.98	56
γ-$LiAlO_2$		3.2[f]	0.7[f]	2.60	1.157	0.69	57
Li-ABW		2.85[g]	0.42[g]	1.45	0.670	0.58	58
sillimanite		6.77[h]	0.532[h]	3.63	1.469	0.65	59

[a] The nonequivalent AlO_4 tetrahedra are indexed according to the structure references. [b] Experimental quadrupole coupling parameters. [c] Mean bond angle deviation calculated from eq 5. [d] Parameters calculated from eq 7 giving an estimate of the geometrical dependency of the EFG tensor. [e] Values from ref 10. [f] Values from ref 46. [g] The C_Q, η values for Li–ABW ($LiAlSiO_4 \cdot H_2O$) are taken from ref 47. [h] The C_Q and η values for sillimanite (Al_2SiO_5) are taken from ref 48.

a minor amount was detected by differential scanning calorimetry. Taylor[25] has suggested that the monosulfate phase could be incorporated within the amorphous calcium silicate hydrate, perhaps interstitified within or near the silicate layers. In consequence, the monosulfate could not only be less ordered in terms of XRD analysis but also exhibit somewhat different thermal behavior compared to synthetic monosulfate. Such differences in the character of the monosulfate could well explain why this phase is so difficult to identify by the above techniques. ^{27}Al MAS NMR therefore appears to have a distinct advantage over these more conventional techniques in detecting and analyzing such aluminate hydrates in complex cryptocrystalline–amorphous environments.

Finally, we note that in the ^{27}Al MAS NMR spectra of both hydrated Portland cements broad resonances are observed in the region for tetrahedrally coordinated Al, which reflects the presence of unhydrated C_3A. The lack of singularities, shoulders, and edges from C_3A has been observed in high-speed spinning ^{27}Al MAS NMR spectra of several unhydrated Portland cements, which indicates that C_3A is not present in a highly crystalline form. This is in agreement with the typical composition of C_3A in Portland cement clinkers, which can contain considerable amounts of Fe_2O_3 (5.1% (w)), SiO_2 (3.7% (w)), MgO (1.4% (w)), and Na_2O (1.0% (w)).[25] Obviously, these impurity ions influence the appearance of the ^{27}Al resonances from the C_3A phase in Portland cement. Furthermore, it is noted that the ferrite phase ($Ca_2(Al_xFe_{1-x})_2O_5$ $0.0 \le x \le 0.7$) is extremely difficult to detect by ^{27}Al MAS NMR because of its high Fe^{3+} content.

Assignment of ^{27}Al Quadrupole Coupling Constants. The relatively large variation in ^{27}Al quadrupole coupling parameters, determined for the anhydrous calcium aluminates in this study, suggests that C_Q and η may be valuable parameters for characterization of the environments of the individual Al sites within the crystal structures of these compounds. C_Q and η depend on the electric field gradients (EFG's) at the nuclear site and appear to be very sensitive to deviations in the local symmetry of the Al sites from ideal octahedral or tetrahedral coordination. The quadrupole coupling constant, which is proportional to the principal component (V_{zz}) of the EFG tensor, is expected to increase with increasing distortion of the coordination polyhedron. Various geometrically dependent parameters have been proposed to describe/quantify the distortion of the coordination polyhedra from perfect symmetry. These parameters include the mean bond angle, bond angle variance, shear strain, and quadratic elongation,[42-45] all of which have been used in correlations with experimental C_Q values for some quadrupolar nuclei in providing tentative assignments for C_Q of individual sites in compounds containing nonequivalent sites.[43-45] In an investigation on the correlation between ^{27}Al C_Q data and polyhedral distortion of the first coordination sphere in a number of minerals, Ghose and Tsang[43] concluded that C_Q is more sensitive to bond angle variations as compared to changes in the Al–O bond length for AlO_4 sites.

Bond angle distortions may be quantified by the mean deviation (D) of the O–Al–O bond angles (θ_i) from the ideal value (θ_T = 109.47°) for a perfect tetrahedron as defined by

$$D = \frac{1}{6}\sum_{i=1}^{6}|\theta_i - \theta_T| \qquad (5)$$

This parameter has been previously employed[44] in interpretations of ^{17}O quadrupole coupling constants, using the assumption that increasing D corresponds to an increase in C_Q. To assign the C_Q values for CA_2, $C_{12}A_7$, and C_3A, which all contain two nonequivalent AlO_4 tetrahedra in the asymmetric unit, we have calculated D for each crystallographic Al site, using the data reported from X-ray diffraction studies. From the C_Q values determined for a few other compounds, which contain only a single AlO_4 tetrahedron in the asymmetric unit (γ-$LiAlO_2$,[46] β-$LiAlO_2$,[10] Li–ABW,[47] and sillimanite[48]), it is observed that C_Q increases with increasing D (cf., Table II and Figure 16a). By the employment of this relationship, the assignment of the C_Q values to the individual sites Al in CA_2, $C_{12}A_7$, and C_3A given in Table II is obtained. Assuming a linear relationship between C_Q and D for all compounds listed in Table II, the correlation

$$C_Q\,(\text{MHz}) = 1.44\,D\,(\text{deg}) + 0.38;\ R = 0.94 \qquad (6)$$

is obtained (Figure 16a). Alternatively, bond angle distortions may be described by the shear strain ($|\psi| = \sum_{i=1}^{6}|\tan(\theta_i - \theta_T)|$)[43] or the bond angle variance ($\sigma_\theta^2 = \sum_{i=1}^{6}(\theta_i - \theta_T)/5$). Using $|\psi|$ and σ_θ^2 as the correlation parameters for the C_Q values of the AlO_4 tetrahedra in Table II, similar correlation coefficients (R) are obtained. Furthermore, both parameters lead to identical assignments of the C_Q values for CA_2, $C_{12}A_7$, and C_3A as obtained using the D values.

Improved insight into the relationship between structure and quadrupole coupling parameters may be obtained by evaluation of the EFG tensors (V) at the nuclear sites from MO calculations.[49,50] However, a simple estimate of the geometrical dependence of V may be arrived at using the approach of Villa and Bjorkstam[51] (i.e., without the need of MO calculations).

(42) Robinson, K.; Gibbs, G. V.; Ribbe, P. H. *Science* **1971**, *172*, 567.
(43) Ghose, S.; Tsang, T. *Am. Mineral.* **1973**, *58*, 748.
(44) Turner, G. L.; Chung, S. E.; Oldfield, E. *J. Magn. Reson.* **1985**, *64*, 316.
(45) Kunwar, A. C.; Thompson, A. R.; Gutowsky, H. S.; Oldfield, E. *J. Magn. Reson.* **1984**, *60*, 467.
(46) Müller, D.; Gessner, W.; Scheler, G. *Polyhedron* **1983**, *2*, 1195.
(47) Jacobsen, H.; Norby, P.; Bildsøe, H.; Jakobsen, H. In preparation.
(48) Raymond, M.; Hafner, S. S. *J. Chem. Phys.* **1970**, *53*, 4110.
(49) Edwards, J. C.; Zubieta, J.; Shaikh, S. N.; Chen, Q.; Bank, S.; Ellis, P. D. *Inorg. Chem.* **1990**, *29*, 3381.
(50) Huggins, B. A.; Ellis, P. D. *J. Am. Chem. Soc.* **1992**, *114*, 2098.
(51) Villa, M.; Bjorkstam, J. L. *J. Magn. Reson.* **1983**, *51*, 349.

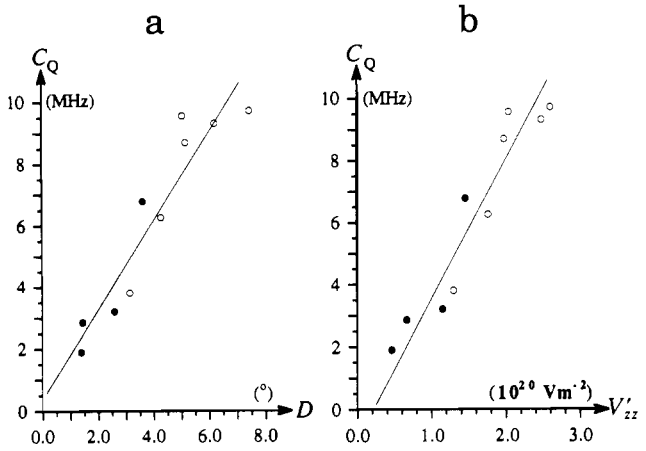

Figure 16. Linear correlations between ^{27}Al quadrupolar coupling constants (C_Q) and (a) the mean bond angle deviation (D) from perfect tetrahedral symmetry and (b) a calculated estimate of the geometrical dependency of the EFG tensor (V'_{zz}) (c.f., eq 7). Open circles represent values for the calcium aluminates CA_2, C_3A, and $C_{12}A_7$, while the filled circles correspond to values for the tetrahedral Al sites in β-$LiAlO_2$, γ-$LiAlO_2$, Li-ABW, and sillimanite. The C_Q, D, and V'_{zz} values used in parts a and b are given in Table II.

These authors considered two contributions to the EFG tensor at the nuclear Al site: (i) a covalent term from the aluminum 3*p* orbitals and (ii) an ionic term from the negative charges of the oxygen atoms.[51] Both contributions include the term $\nabla\nabla\boldsymbol{R}_i^{-1}$, where $\mathbf{R}_i$ is the modulus of the Al–O_i internuclear vector, and an estimate ($\boldsymbol{V}'$) of the geometrical dependence of the EFG tensor may be obtained by the summation

$$\boldsymbol{V}' = \frac{e}{4\pi\epsilon_0}\sum_{i=1}^{4}\nabla\nabla\boldsymbol{R}_i^{-1} \qquad (7)$$

over the four oxygen atoms within the first coordination sphere of the Al atom. It is noted that this approach corresponds to a point–monopole calculation,[52] where only the oxygen ions in the first coordination sphere are taken into account. The elements of the $\boldsymbol{V}'$ tensor in eq 7 are calculated from the reported crystal structures and the principal components ($|V'_{zz}| \geq |V'_{yy}| \geq |V'_{xx}|$) are obtained by diagonalization of the $\boldsymbol{V}'$ tensor. The principal element (V'_{zz}) and the EFG asymmetry parameter ($\eta' = V'_{xx} - V'_{yy})/V'_{zz}$) calculated for the anhydrous calcium aluminates as well as for γ-$LiAlO_2$, β-$LiAlO_2$, Li-ABW, and sillimanite are listed in Table II. For the compounds containing a single AlO_4 site, V'_{zz} is found to increase with increasing C_Q. The assignment of C_Q for the nonequivalent Al sites in CA_2, $C_{12}A_7$, and C_3A, based on this relationship, is identical to the assignment obtained from the D values. The linear correlation between V'_{zz} and C_Q for the above samples is illustrated in Figure 16b and corresponds to

$$C_Q\,(\mathrm{MHz}) = 4.03V'_{zz}(\times 10^{20}\ \mathrm{V/m^2}) - 0.23;\ R = 0.95 \qquad (8)$$

While the V'_{zz} parameters correlate well with the observed quadrupole coupling constants, the calculated η' values are not in such good agreement with the η values determined experimentally for some of the samples listed in Table II. The assignment of the C_Q data for CA_2, $C_{12}A_7$, and C_3A has been further confirmed by Gaussian 90 MO calculations[53] on AlO_4^{5-} tetrahedra,[54] employing the *D95* basis set[50] and the specific geometry of each AlO_4 tetrahedron in these aluminates. The above correlations should allow examination of whether the tentative C_Q values determined for CA are consistent with its crystal structure.[27] Unfortunately, using the atomic coordinates for CA[27] and the ORTEPII program package,[55] we found it impossible to reproduce the interatomic distances and angles reported in that paper.[27] This precluded an analysis of the C_Q values for CA in terms of the above correlations and thus to predict the C_Q values to occur in subgroups of three, two, and one (Table I) as determined experimentally.

Although only atoms in the first coordination shell are considered, valuable relationships between C_Q and the distortion of the AlO_4 tetrahedra are observed. D and V'_{zz} appear to be useful parameters for describing the distortion of AlO_4 tetrahedra and in assignment of C_Q values to AlO_4 sites (eqs 6 and 8). The improved correlation observed between C_Q and V'_{zz}, compared to C_Q versus D, may reflect that V'_{zz} includes variations in bond angles as well as bond lengths. This is in full agreement with MO calculations of ^{95}Mo C_Q values for octahedrally coordinated Mo, which show that variations in bond angles and bond lengths within the first coordination sphere, have a considerable influence on the C_Q values.[49] Further insight into the relationship between quadrupole coupling parameters and structure, as well as, the prospects of extracting the maximum information from C_Q and η, obviously requires that charge distributions from further distant coordination spheres are considered. However, we believe that this work has proven that reasonably good predictions of the magnitude of C_Q for AlO_4 tetrahedra (at least for the compounds considered here), may be obtained by considering only the first coordination sphere and employing the C_Q versus D and V'_{zz} correlations in eqs 6 and 8.

Conclusion

The ^{27}Al MAS NMR studies in this investigation, of synthetic calcium aluminates and aluminate hydrates, as well as hydrated high alumina and Portland cements, have shown the great potential of this technique in studies of cementitious systems. For the synthetic phases optimum sets of the quadrupolar coupling constants (C_Q) and asymmetry parameters (η) (or the *SOQE* parameters) have been obtained from ^{27}Al MAS NMR spectra in combination with numerical simulation/optimization procedures. For strong ^{27}Al quadrupolar couplings ($C_Q \cong 4$–12 MHz), these parameters are most conveniently determined by simulation of undistorted line shapes for the central transition and its ssb's observed in high-speed ($\nu_r \cong 10$–18 kHz) spinning ^{27}Al MAS spectra. For weak and intermediate quadrupole interactions ($C_Q \cong 0.3$–4 MHz), simulations of the complete manifold of ssb's observed for the satellite transitions represents a superior method for determination of C_Q and η with high accuracy. Furthermore, it is demonstrated that moment analysis of ^{27}Al MAS NMR spectra of very weak quadrupole interactions ($C_Q \lesssim 0.5$ MHz) allows the *SOQE* parameter to be determined with improved accuracy, compared to the usual method employing second-order quadrupolar shifts of the individual transitions.

From the C_Q, η, and δ values for the synthetic phases it is observed that variations in the local electronic structure and the geometry of the Al coordination polyhedra are strongly reflected by the quadrupolar coupling parameters, while only minor variations in the δ values are observed within the chemical shift regions for Al(4) and Al(6). Thus, the quadrupolar coupling parameters are very important for the identification/characterization of the individual Al components in "real" cements, as

(52) Cohen, M. H.; Reif, F. *Solid State Phys.* **1957**, *5*, 321.
(53) GAUSSIAN 90, Revision F: Frisch, M. J.; Head-Gordon, M.; Trucks, G. W.; Foresman, J. B.; Schlegel, H. B.; Raghavachari, K.; Robb, M.; Binkley, J. S.; Gonzales, C.; Defrees, D. J.; Fox, D. J.; Whiteside, R. A.; Seeger, R.; Melius, C. F.; Baker, J.; Martin, R. L.; Kahn, L. R.; Stewart, J. J. P.; Topiol, S.; Pople, J. A. Gaussian, Inc., Pittsburgh, PA, 1990.
(54) Skibsted, J.; Jakobsen, H. J.; Ellis, P. D. Unpublished results.
(55) Johnson, C. K. ORTEPII. Report ORNL-5138. Oak Ridge National Laboratory, Oak Ridge, TN, 1976.
(56) (a) Marezio, M. *Acta Crystallogr.* **1965**, *18*, 481. (b) JCPDS powder diffraction file No. 33-785.
(57) Marezio, M. *Acta Crystallogr.* **1965**, *19*, 396.
(58) Krogh Andersen, E.; Plough-Sørensen, G. *Z. Kristallogr.* **1986**, *176*, 67.
(59) Winther, J. K.; Ghose, S. *Am. Mineral.* **1979**, *64*, 573.

illustrated by the ^{27}Al MAS spectra of hydrated samples of high alumina and Portland cements. With the exception of ettringite ($C_6A\bar{S}_3H_{32}$), the C_Q, η, and δ values are in agreement with the reported crystal structures. The ^{27}Al MAS NMR spectra of ettringite have demonstrated that all Al^{3+} ions are in equivalent positions in the asymmetric unit, which is not consistent with the crystal structure determined by Moore and Taylor,[37] who reported two nonequivalent Al sites in the unit cell. For C_4AH_{13} and monosulfate ($C_4A\bar{S}H_{12}$), the observed ssb patterns from the satellite transitions cannot be described by a single set of C_Q, η values, but rather by a distribution in these parameters. This distribution is estimated by simulated ssb manifolds, employing ca. 10 sets of slightly different C_Q and η values, which probably reflects small structural anomalies such as disorder or dynamic processes within these hydrates. For the anhydrous calcium aluminates, the observed C_Q values may be related to the distortion of the AlO_4 tetrahedron, which in this study are quantified using the mean bond angle deviation from perfect tetrahedral symmetry and a calculated estimate of the geometrical dependency of the EFG tensor. Reasonably good correlations between these parameters and the C_Q values are observed, even though only effects from the first coordination sphere are considered. These correlations allow assignment of the C_Q values for the calcium aluminates, CA_2, $C_{12}A_7$, and C_3A, each containing two nonequivalent AlO_4 tetrahedra in the asymmetric unit.

^{27}Al MAS NMR studies of hydrated high alumina and Portland cements have shown that detailed information about the formation and consumption of the individual Al species in "real" cements can be obtained using this technique. The ssb manifolds from satellite transitions have been found to be useful for identification of the individual Al components and can also provide information about the degree of crystallinity of such phases in cements. From a spectrum of hydrated high alumina cement (hydrated for 28 days), C_3AH_6 and AH_3 were found to be the dominating Al phases; however, minor amounts of unhydrated CA and CA_2 were also observed. Despite a chemical shift difference of only 1.3 ppm between ettringite and monosulfate, these phases are distinguished in the high-resolution ^{27}Al MAS NMR spectra of ordinary Portland cement hydrated for 28 days. Ettringite is easily identified from the observed manifold of ssb's and is present as the main hydrated Al phase after hydration for one day. The relative proportions of ettringite and monosulfate in the sample hydrated for 28 days has been calculated by deconvolution of the central transition centerband intensities.

Acknowledgment. The authors wish to thank Lafarge Coppee Recherche, Viviers, France, and Aalborg Portland A/S, Aalborg, Denmark, for providing some of the samples used in this study. We are grateful to Drs. Rita and Alan Hazell for the drawings of the structures for CA_2 and ettringite and for their assistance with the ORTEP calculations. The use of the facilities at the University of Aarhus NMR Laboratory sponsored by Teknologistyrelsen, the Danish Research Councils (SNF and STVF), Carlsbergfondet, and Direktør Ib Henriksens Fond is acknowledged. J.S. thanks the SNF (11-9160) for financial support.